EFFECTS OF ACCELERATION, DECELERATION, AND CORNERING ON OCCUPANTS INSIDE A HYPERLOOP CAPSULE/POD AT SUPERSONIC VELOCITIES

A Thesis by

Sandeep Vijayan

Bachelor of Engineering, Visvesvaraya Technological University, 2013

Submitted to the Department of Mechanical Engineering
and the faculty of the Graduate School of
Wichita State University
in partial fulfillment of
the requirements for the degree of
Master of Science

December 2017

EFFECTS OF ACCELERATION, DECELERATION, AND CORNERING ON OCCUPANTS INSIDE A HYPERLOOP CAPSULE/POD AT SUPERSONIC VELOCITIES

The following faculty members have examined the final copy of this thesis for form and content, and recommend that it be accepted in partial fulfillment of the requirement for the degree of Master of Science with a major in Mechanical Engineering.

_____

Hamid Lankarani, Committee Chair

_____

Krishna Krishnan, Committee Member

_____

Rajeev Nair, Committee Member

DEDICATION

To my beloved family (Vijayan, Prabha, Shriyaadita, Shrivardhan)

To my advisor, Dr. Hamid Lankarani (Dr. L.)

“Mano buddhi ahankara chittani naaham

na cha shrotrajihve na cha ghraana netre

na cha vyoma bhumir na tejo na vaayuhu

chidananda rupah shivo’ham shivo’ham”

I am not the mind, the intellect, the ego or the memory,

I am not the ears, the skin, the nose or the eyes,

I am not space, not earth, not fire, water or wind,

I am the form of consciousness and bliss,

I am the eternal Shiva…

ACKNOWLEDGMENTS

I hereby extend my heartfelt gratitude to Dr. Lankarani, Professor at the Department of Mechanical Engineering, for mentoring me through the entire course of my master's program. Without whose unwavering support, guidance, and enthusiasm, writing this thesis would never be possible. I offer my sincere appreciation for all the learning opportunities that was provided to me. I wish you would continue molding students the way you do and help them go beyond their limits.

My heartfelt thanks to Dr. Krishna Krishnan and Dr. Rajeev Madhavan Nair for agreeing to be a part of my committee and for their valuable time spent in reviewing this thesis.

Ancestors who paved the path before me upon whose shoulders I stand. My parents, for being there through thin and thick, and for the unconditional love. I thank you as writing this thesis wouldn't be possible without your presence in my life.

Finally, my thanks to all the friends who have been a part of the whole master's journey. Special thanks to D.V. Suresh K, for all the support and help which played a crucial role in completing this thesis.

ABSTRACT

Living in an era when commuting at supersonic velocities is all set to transform into reality, the safety of an occupant is of paramount significance to the transportation provider or the manufacturer. The Hyperloop, a fifth mode of transportation proposed by Mr. Elon Musk is progressing towards complete realization. An occupant traveling in a Pod/Capsule inside a partial vacuum tube at supersonic speeds might have to deal with extreme G-forces, at times greater than that experienced by pilots of jet aircrafts. Computer simulations have facilitated the analysis of forces acting on a dummy/Human body model in various scenarios. This thesis presents an investigation into the consequential effect of various parameters on the G-forces acting on the occupant and determining proper restraint systems and seating configurations. A Hybrid-III and a EuroSID-2re 50th percentile male dummies are made use of in the occupant modeling code MADYMO under various test conditions. Computer simulations are carried out to determine the kinematics, injury pass/fail criteria, belt forces during acceleration, deceleration and while the capsule travels along a curved path, of a radius of curvature one mile. For each input test condition, three seat configurations are considered, and each seat configuration is computationally tested with three restraint system configurations and one without any kind of restraint system. At the end of the study, an optimal seat and restraint system configuration are identified after careful examination of results.

TABLE OF CONTENTS

Chapter **Page**

TABLE OF CONTENTS (continued)

Chapter **Page**

LIST OF TABLES

Table **Page**

LIST OF TABLES (continued)

Table **Page**

LIST OF FIGURES

LIST OF FIGURES (continued)

Figure **Page**

ABBREVIATIONS

MADYMO	Mathematical Dynamic Model
HIC	Head Injury Criterion
FAA	Federal Aviation Administration
MATLAB	Matrix Laboratory
ADAMS	Automated Dynamic Analysis of Mechanical Systems

CHAPTER ONE
INTRODUCTION

1.1 Background

Transportation systems have evolved after going through various trials and tribulations, just like the evolution of human kind. It has grown by overcoming all challenges, to levels of complexity that is ever-increasing. Mankind has come a long way, be it walking during the Stone Age to the complex and efficient modes of transportation that we currently enjoy. All new concepts have been overlooked with skepticism, some prevailed and some vanished. The journey has been long. As the world gets more competitive and time becomes more precious than ever, the urge to reduce commuting time efficiently has sky-rocketed. As a result, various attempts have been made to come up with concepts and faster working alternative to conventional modes of transportation.

A conceptual transportation system intended to bring down travel time and travel expenses was proposed by Elon Musk and a group of specialists from Tesla Motors and the Space Exploration Technologies Corporation (SpaceX) on August 2013 as an open plan to be checked, refined and transformed into a practical reality. The idea is to deviate from existing conventional rail systems by disposing of the rails, the passenger is enclosed in a capsule or pod which moves through a tube maintained at a low pressure, partial vacuum condition. The capsule is suspended by means of air bearings or by magnetic levitation [1]. The tubes through which the Hyperloop pod travels would be elevated from ground level with the use of pylons as illustrated in Figure 1.1 or other supporting structures spaced about 100 meters away from each other. The Hyperloop is expected to carry passengers from Los Angeles to San Francisco in about 35 minutes and is expected to attain speeds close to 750mph, which would be ground breaking the field of transportation.

Figure 1.1 Illustration the tube, pylons, and the pod [17].

Hyperloop being an open concept various startup companies have taken up the task of deploying the technology and advance it further. Hyperloop One, Arrivo and Hyperloop Technologies are the startups that has had its share of research, facility building, and capital raising to transform the concept into reality. Rumor has it that Mr. Elon Musk himself has plans of building his own Hyperloop, which is yet to be confirmed. Figure 1.2 shows the pod designed and built by Hyperloop One. This pod has undergone a full-scale test in partial vacuum conditions, nearly hitting 200mph

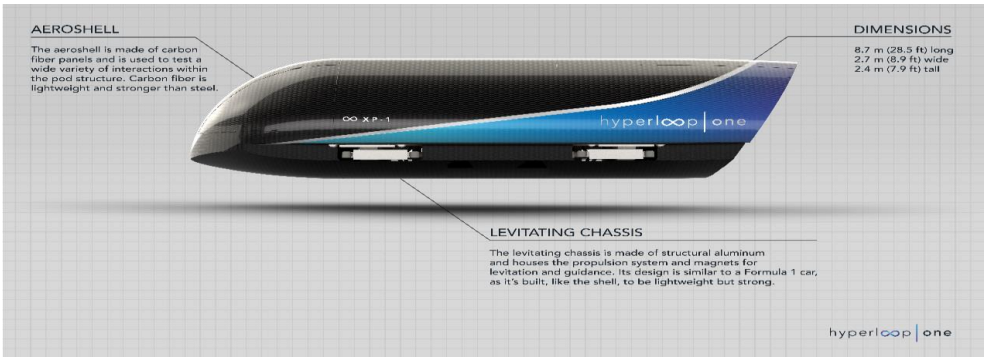

Figure 1.2 Pod designed and built by Hyperloop technologies [18]

1.2 Literature Review

Chin [1], discussed in depth about the concept called Hyperloop, various design possibilities, probable dimensions, etc. A study by Taylor, discussed about the commercial feasibility of the Hyperloop [7], the study also laid out few interesting questions regarding depressurization situation, stranded pod, excessive drag, and capsule behavior at supersonic velocities, how long the pod would continue to run in the event of power loss and so on.

Head injury due to linear acceleration was spoken about in detail by King and Rowson [2, 3]. King's study [2] had detailed description of brain injury mechanisms, role of linear and rotational accelerations, concussion mechanisms and probability of head linear injury. Viano's [4] study debates about the requirement for precise information on translational and rotational acceleration experienced by the head as the primary step for evaluating the Head injury criteria (HIC) [24].

Ewing [5] deals mostly with measurement of responses of T1, head and pelvis to -Gx impact acceleration and describes the propagation of the acceleration profile from pelvis to T1 to the head. The utilization of these information for depiction of the entire dynamic reaction of man has been discussed. Ewing [6] considers dynamic response due to +Gy impact on human neck and head and compares time profiles of linear resultant acceleration, angular acceleration, and angular velocity at the anatomical origin of the head and horizontal linear acceleration linear acceleration at the origin of T1 and exhibited at chosen categorized peak acceleration levels for 5 subjects of different anthropometric dimensions.

Lankarani [9] [10] [11] [12] [13], has conducted extensive research in various injury criteria, lumbar loads, aircraft crash injury protection and so on, prominent few of which pertaining

to this study has been reviewed and mentioned here. Lankarani [12], Sheds light on computer simulation possibilities in an occupant-restraint system, reference [14] provides strong foundation to this study.

Osth [7] provided an insight on how occupants respond to autonomous Deceleration. Though this paper dealt with human body models and emphasis was on musculature, the general information about occupant response was of great benefit.

Tay [9], estimated lumbar loads for a Hybrid-III scalable dummy based on numerous FAA regulations in the event of a crash. In this study tolerance of lumbar load values for the 5th and 95th percentiles are proposed to be 870 lb. (3,871 N) and 1772 lb. It also presented a comparison of lumbar load tolerances with other sources.

Zhang [20], used kriging model-based optimization in order to generate surface response data using selected sample input data from ADAMS simulations, which helped predicting the influence of design parameters on clearance in a revolute joint. And also reducing the number of simulations. Prasanna [21], dealt with generation of response surface data of HIC associated with various aircraft and automotive scenarios, utilizing a kriging model built based on a few input parameters obtained from various MADYMO simulations.

Prabhu [15], probed into the head path and HIC of occupants in a passenger aircraft utilizing the Federal Aviation Regulation (FAR) Part 25 and Part 23 and showed how HIC and the head path varied in different scenarios. His objective was to find optimal bulkhead stiffness and a set of parameters which would greatly help reduce the fatalities in an aircraft accident. Tass International [16] provided all necessary instructions on making complete use of Occupant modelling code MADYMO.

1.3 Motivation

Hyperloop being the technology that can revolutionize the transport industry, has extensive research being conducted on the technology. Questions have been asked on safety of the Hyperloop ever since the inception of the concept. What would happen on an event of power loss, depressurization, pod getting stranded, minimizing drag at supersonic velocities, etc., are few of the prominent questions being asked. After reviewing few papers, it was evident that there has not been enough emphasis on safety of the occupant inside the pod. The occupant is locked inside a capsule which is expected to accelerate to supersonic velocities in minimal time. In such a case an occupant would definitely undergo way more G-forces than the tolerable limit. And also decelerating from high speeds would cause the occupant to be displaced from the seat, in the absence of appropriate safety restraints.

There were few curved paths along the proposed route between LA and San Francisco. This raises a question of what the ideal turning radius would be and also what would be the impact of lateral acceleration on the occupant along a path with of smaller turning radius. The curiosity to know the effects of such rapid acceleration on an occupant has provided the motivation to probe deeper into the issue and examine the influence of different seating and belt configuration during acceleration, deceleration and cornering scenarios, on injury criteria and the kinematics itself.

Various seating and restraint conditions can be assumed and injury probabilities, and the basic kinematics behavior can be analyzed using occupant modelling packages such as MADYMO. And by utilizing a kriging model-based optimization surface plots can be generated using selected input parameters, which would be very beneficial for anyone utilizing this study for designing purposes.

CHAPTER TWO
OBJECTIVES AND METHODOLOGY

2.1 Objectives

Occupant safety inside the Hyperloop pod forms the basis of this study. This study basically focusses on:

- Evaluation of kinematics, various injury criteria, belt loads acting on an occupant inside a Hyperloop capsule utilizing various seating and belt configurations and compare them under various acceleration, deceleration and cornering scenarios.
- Development of design charts using Kriging Model-Based Optimization.
- Arriving at the optimal seating and restraint system configurations based on the results obtained.

2.2 Methodology

Modelling was done using MADYMO, a multibody occupant safety system widely used in the aircraft and the automotive industry. Product modules such as XMADgic, xml editor used to edit the input deck and MADpost, post processor. A basic model was developed in MADYMO and various modifications were made to obtain the required seat configuration. Hybrid-III and EuroSID-2re 50th percentile male dummies have been made use of throughout the study. Appropriate dummy was imported and adjusted as per requirement of specific configurations. Three different seat configurations are created by modifying the basic model created. FE belts were created using belt fitting tool. 2-point configuration which consists of a lap belt, 3-point configuration which consists of a shoulder belt and a lap belt, 4-point configuration which consists

of two shoulder and one lap belt were created tested with each seating configuration. Three different test conditions were employed. Velocity and the time take to attain the same were utilized to calculate the acceleration value.

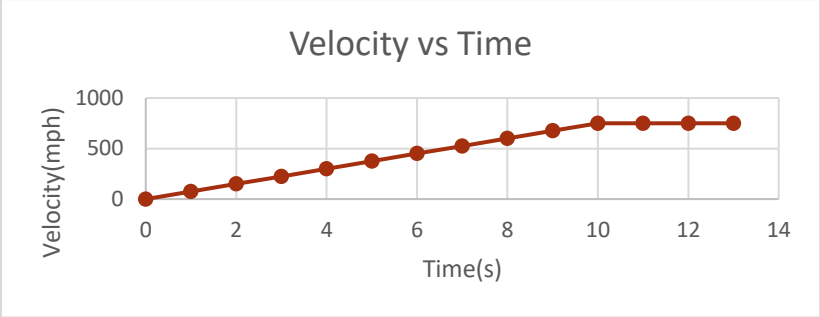

Figure 2.1 Sample Velocity vs Time graph

Constant acceleration has been considered in all cases for this study. It is shown in the Figure 2.1. Acceleration was calculated using:

$$a = \frac{\Delta v}{\Delta t} \tag{2.1}$$

$$a = \text{Acceleration}, \Delta v = \text{Change in Velocity}, \Delta t = \text{Time taken}$$

The g-forces acting on the occupant is therefore determined. Acceleration and Deceleration scenarios were mimicked in MADYMO by applying a constant acceleration value along positive and negative direction of the axis along which the dummy is oriented.

The configurations were computationally tested in various acceleration, deceleration and cornering conditions. The acceleration pulse obtained from each test condition is applied to the occupant in various seating and restraint system configuration, to examine the kinematic behavior of the occupant. Few other parameters like head acceleration, pelvic acceleration and other injury pass/fail criteria are tabulated and examined.

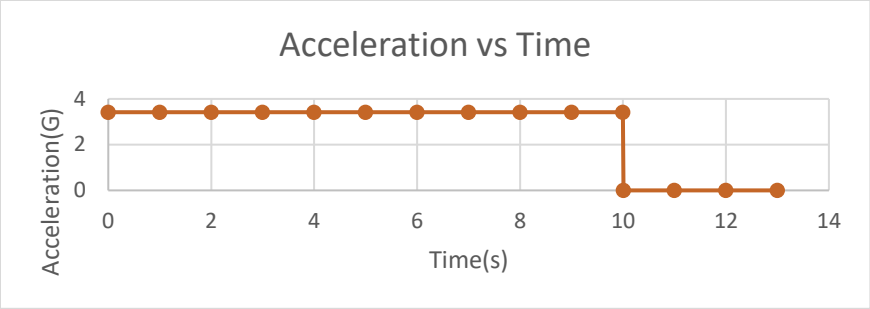

Figure 2.2 Acceleration in G corresponding to the above velocity vs time graph

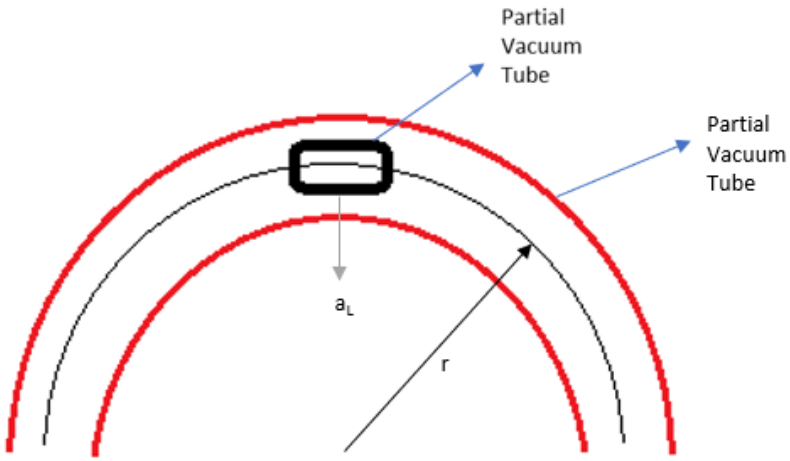

Figure 2.3 Representation of a Hyperloop Capsule/Pod travelling along a curved path

While travelling along a curved path, the pod experiences a lateral acceleration, Figure 2.2. For this study, a one-mile radius of curvature is considered for the curved path taken by the pod, using which the lateral acceleration is calculated. The lateral acceleration was calculated using:

$$a_L = \frac{v^2}{\rho} \tag{2.2}$$

a_L = Lateral Acceleration, $v = Velocity$, $\rho = Radius\ of\ Curvature$

Table 2.1 Lateral Acceleration at Different Radii of Curvature

Radius of Curvature (ρ)	Velocity (v)	Lateral Acceleration (a_L)
1-mile	210mph	0.6G
	750mph	7.1G
5-mile	210mph	0.1G
	750mph	1.4G
10-mile	210mph	0.05G
	750mph	0.7G

Calculations were made using various radii of curvature and velocities, lateral acceleration corresponding to the same are recorded in the Table 2.1. It can be observed from the table that the values of lateral acceleration obtained for five-mile and ten-mile radii of curvature, at both the considered velocities are significantly lower. Therefore, to analyze the cornering effect in an extreme case a one-mile radius of curvature has been considered for this study. Lateral acceleration value for one-mile radius of curvature at 210mph is observed to be a much smaller value. And since the Hyperloop is expected to travel at speeds of 700-750mph, a velocity of 750mph has been considered for this study. Therefore, the lateral acceleration value corresponding to one-mile radius of curvature and 750mph velocity has been considered.

Lateral acceleration 7G is applied to all cornering cases throughout the study. The lateral acceleration calculated was applied to the dummy along positive y-direction in MADYMO to replicate the scenario of cornering along a curved path, and analyzed while in different seating and restraint system configurations for test conditions A and B.

2.2.1 Test Condition – A (Slower Acceleration-Tesla Branded Pod)

During a recent test the Tesla-branded Hyperloop pod achieved a speed of 210mph in 15 seconds. The first Test condition considered for this study is obtained from the same. Constant acceleration has been considered. The velocity vs time graph is shown in the Figure 2.4.

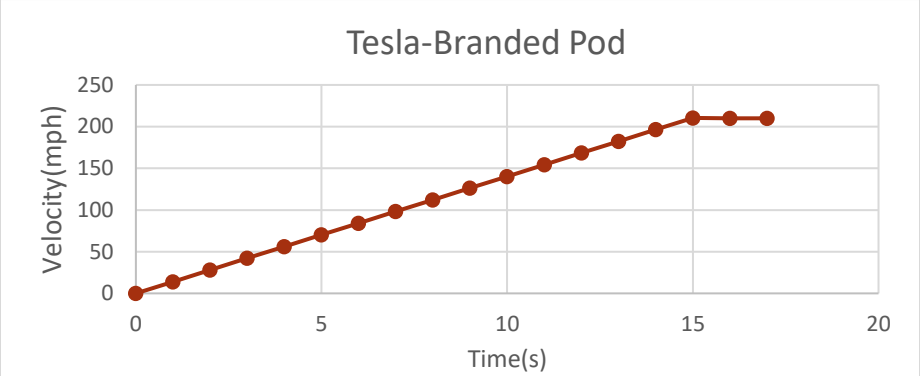

Figure 2.4 Velocity time graph of the Tesla-Branded pod

The acceleration was calculated using Eq.2.1. A constant acceleration of 0.64G was applied on the dummy on positive and negative direction separately, to mimic acceleration and deceleration scenario. A lateral acceleration of 7G along with forward acceleration of 0.64G is applied on the dummy to replicate the motion of the pod along a curved path. Acceleration pulse used in test condition-A is shown in Figure 2.5.

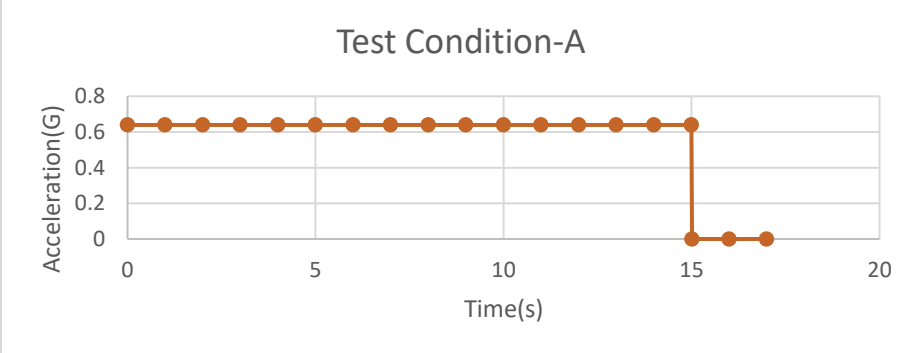

Figure 2.5 Acceleration pulse used in Test Condition-A

2.2.3 Test Condition-B (Rapid Acceleration-Hyperloop Top Speed)

The Hyperloop pod is expected to achieve speeds of the order of 750mph. There is not much information on how fast the pod is expected to attain this speed, a 10-second time span is considered for this study, Figure 2.6.

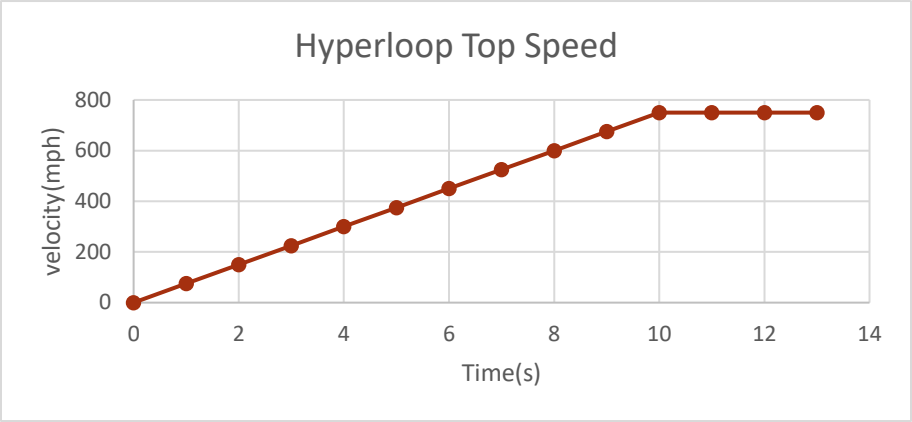

Figure 2.6 Velocity vs Time (750mph in 10-seconds)

Constant acceleration of 3.4G is applied on the dummy, Figure 2.7. Acceleration and deceleration conditions are tested. A lateral acceleration of 7G is applied to the dummy along with forward acceleration to replicate motion along a curved path of radius of curvature one-mile.

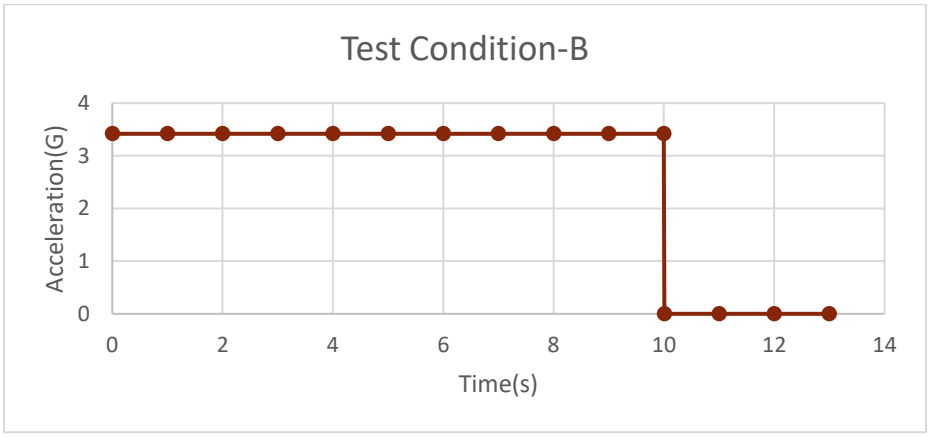

Figure 2.7 Acceleration pulse used in Test Condition-B

2.2.2 Test Condition-C (Worst case)

Dr. John Stapp who was renowned as the “Fastest man on Earth”, for his rocket sled experiments for the US air force, using himself as a test subject. During his final sled run, he is said to have encountered more than 40G. The third test condition used in this study is derived from this sled test. Studying such patterns of acceleration, deceleration and cornering will shed light on the effects on the occupant. In this case the rocket powered sled accelerates from 0 to 632mph in 5 seconds and comes to a complete stop in 1.4 seconds. Constant acceleration is considered in case of acceleration and an ideal triangular pulse is considered in case of deceleration. The graph of which is shown in the Figures 2.8 and 2.9.

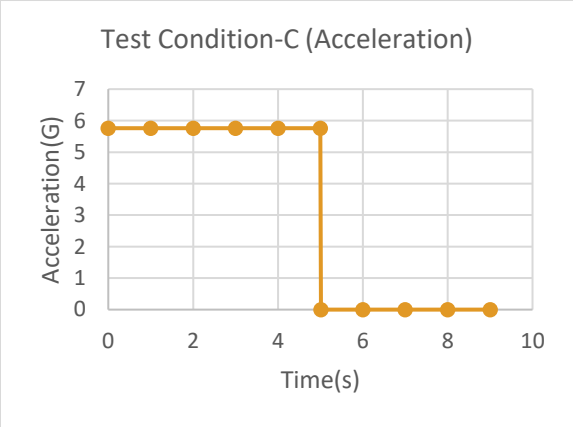

Figure 2.8 John Stapp Acceleration pulse

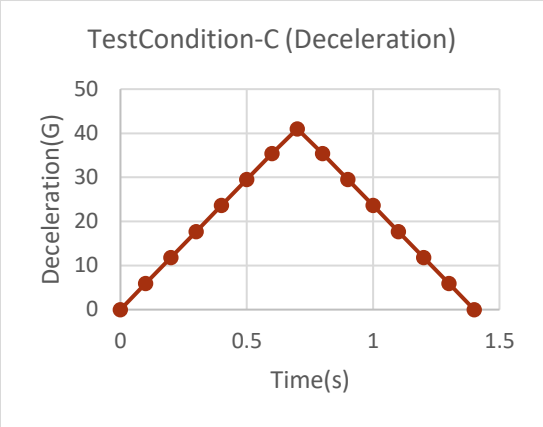

Figure 2.9 John Stapp Deceleration pulse

The kinematics, head acceleration, lumbar resultant forces, pelvis acceleration and belt forces were recorded for each individual configuration of seat, restraint system and acceleration conditions. Frontal and lateral head excursion was recorded in case of deceleration and cornering, respectively. A bulkhead was introduced into the no-belt deceleration scenarios to illustrate what would happen during deceleration without safety restraints.

A flowchart showing the overall methodology is shown in Figure 2.10.

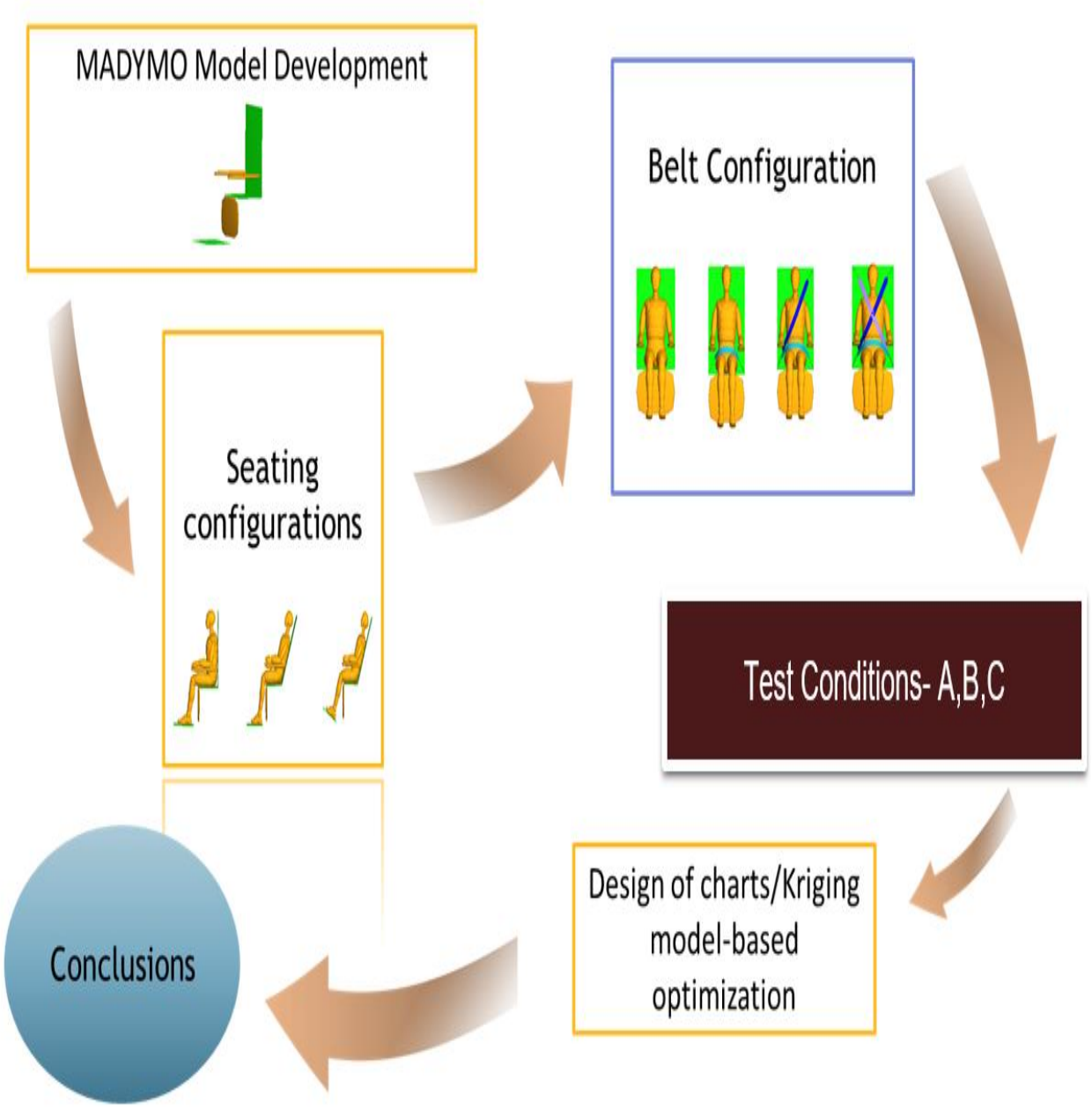

Figure 2.10 a flowchart showing Overall Methodology

All the cases considered in various test conditions are shown in Figures 2.11, 2.12, 2.13. In total 96 cases have been simulated in MADYMO.

Test Condition-A (Slower Acceleration-Tesla Branded Pod)	Acceleration	Seat Configuration-I (Seat-Back angle-90°)	No-belt
			Two-Point
			Three-Point
			Four-Point
		Seat Configuration-II (Seat-Back angle-120°)	No-belt
			Two-Point
			Three-Point
			Four-Point
		Seat Configuration-III (Seat-Back angle-120°) (Sled Floor angle-160°)	No-belt
			Two-Point
			Three-Point
			Four-Point
	Deceleration	Seat Configuration-I (Seat-Back angle-90°)	No-belt
			Two-Point
			Three-Point
			Four-Point
		Seat Configuration-II (Seat-Back angle-120°)	No-belt
			Two-Point
			Three-Point
			Four-Point
		Seat Configuration-III (Seat-Back angle-120°) (Sled Floor angle-160°)	No-belt
			Two-Point
			Three-Point
			Four-Point
	Cornering (Using EuroSID 2re)	Seat Configuration-I (Seat-Back angle-90°)	No-belt
			Two-Point
			Three-Point
			Four-Point
		Seat Configuration-II (Seat-Back angle-120°)	No-belt
			Two-Point
			Three-Point
			Four-Point
		Seat Configuration-III (Seat-Back angle-120°) (Sled Floor angle-160°)	No-belt
			Two-Point
			Three-Point
			Four-Point

Figure 2.11 Test Condition-A, Cases Considered

Test Condition-B (Faster Acceleration-Hyperloop Top speed)	Acceleration	Seat Configuration-I (Seat-Back angle-90°)	No-belt
			Two-Point
			Three-Point
			Four-Point
		Seat Configuration-II (Seat-Back angle-120°)	No-belt
			Two-Point
			Three-Point
			Four-Point
		Seat Configuration-III (Seat-Back angle-120°) (Sled Floor angle-160°)	No-belt
			Two-Point
			Three-Point
			Four-Point
	Deceleration	Seat Configuration-I (Seat-Back angle-90°)	No-belt
			Two-Point
			Three-Point
			Four-Point
		Seat Configuration-II (Seat-Back angle-120°)	No-belt
			Two-Point
			Three-Point
			Four-Point
		Seat Configuration-III (Seat-Back angle-120°) (Sled Floor angle-160°)	No-belt
			Two-Point
			Three-Point
			Four-Point
	Cornering (Using EuroSID 2re)	Seat Configuration-I (Seat-Back angle-90°)	No-belt
			Two-Point
			Three-Point
			Four-Point
		Seat Configuration-II (Seat-Back angle-120°)	No-belt
			Two-Point
			Three-Point
			Four-Point
		Seat Configuration-III (Seat-Back angle-120°) (Sled Floor angle-160°)	No-belt
			Two-Point
			Three-Point
			Four-Point

Figure 2.12 Test Condition-B, Cases Considered

Test Condition-C (Most Severe Case - Hyperloop Top speed)	Acceleration	Seat Configuration-I (Seat-Back angle-90^{o})	No-belt
			Two-Point
			Three-Point
			Four-Point
		Seat Configuration-II (Seat-Back angle-120^{o})	No-belt
			Two-Point
			Three-Point
			Four-Point
		Seat Configuration-III (Seat-Back angle-120^{o}) (Sled Floor angle-160^{o})	No-belt
			Two-Point
			Three-Point
			Four-Point
	Deceleration	Seat Configuration-I (Seat-Back angle-90^{o})	No-belt
			Two-Point
			Three-Point
			Four-Point
		Seat Configuration-II (Seat-Back angle-120^{o})	No-belt
			Two-Point
			Three-Point
			Four-Point
		Seat Configuration-III (Seat-Back angle-120^{o}) (Sled Floor angle-160^{o})	No-belt
			Two-Point
			Three-Point
			Four-Point

Figure 2.13 Test Condition-C, Cases Considered

Since a lateral acceleration of 7G has been applied in case of cornering scenarios. Test condition-C being the most severe case has not been tested in the cornering scenario.

CHAPTER THREE

MODEL DEVELOPMENT

3.1 Basic Model Development

The model representation is developed using planes and ellipsoids, Figure 3.1. The Top seat is a plane of 35 inches in height, 23 inches wide and is fully upright, at right angle to the X-axis. The bottom seat is a plane, 15 inches in length and 23 inches in width. Similarly, the sled floor is a plane, 17 inches in length and 23 inches wide. The arm-rests and bottom-leg are developed using ellipsoids. The armrests are 12 inches in length, 2.4 inches in width and 0.8 inches in height. A bulkhead plane, 35 inches in height and 23 inches in width is made use of in the no-belt deceleration scenarios. The model therefore developed is modified accordingly to obtain the seating configurations required for the study. The seat model representation is shown in Figure 3.2.

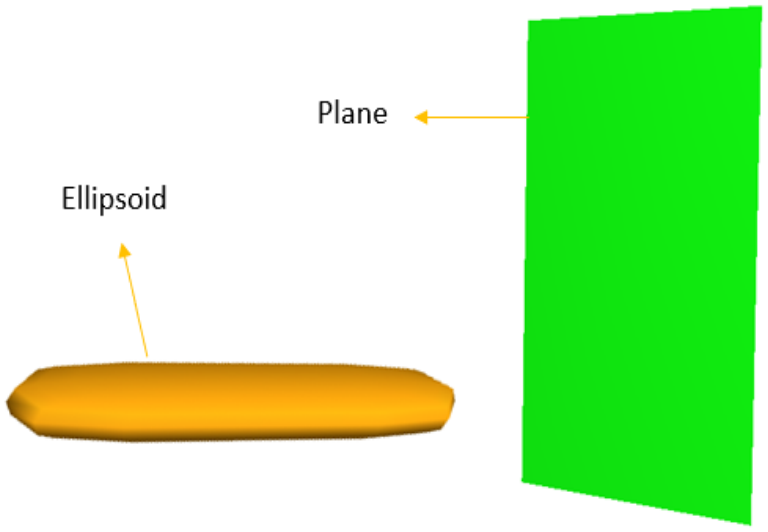

Figure 3.1 Sample Ellipsoid and Plane used to develop the seat model

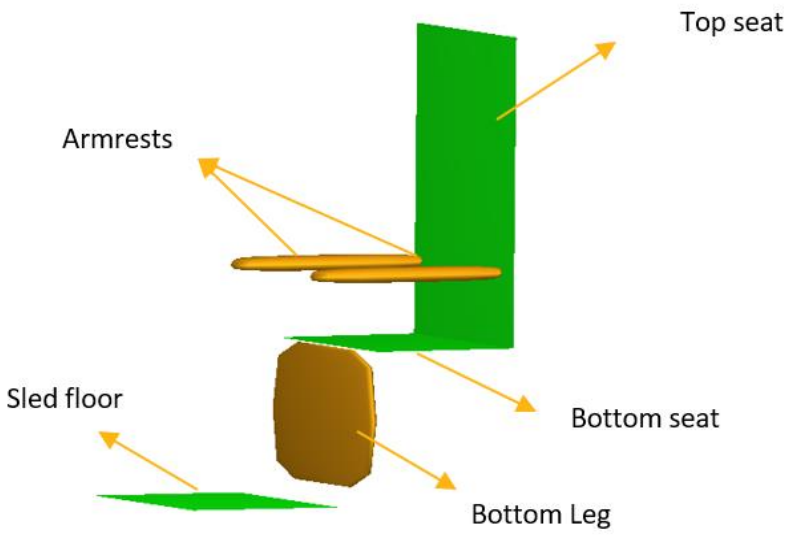

Figure 3.2 The Seat model representation

3.2 Dummy Model

Hybrid III and EuroSID-2re 50th percentile male dummies are made use of throughout the study, Figure 3.2. The Hybrid-III was used in the deceleration and acceleration scenarios, whereas EuroSID was used in the cornering cases.

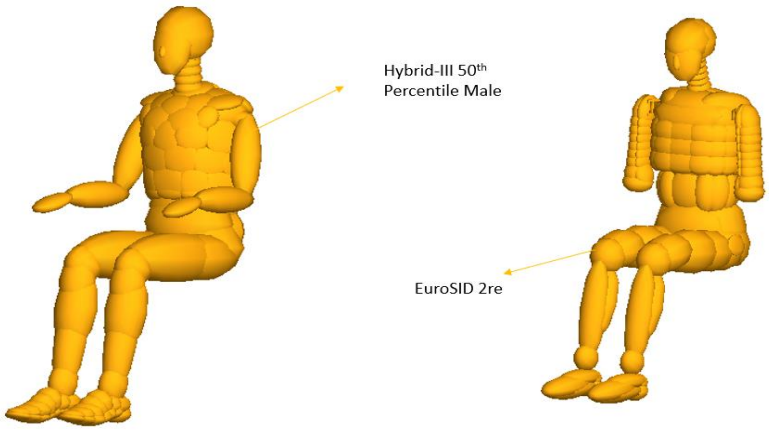

Figure 3.3. Hybrid-III and EuroSID-2re 50th Percentile male dummies

Respective dummies are imported and adjusted as per requirement using the joint positioning tool, Figure3.4. The dummy placed is on the bottom seat and adjusted in such a way that the back rests against the top seat, forearms are positioned on the armrest and feet on the sled floor. The complete representation of the dummy placed on the seat is shown in Figure 3.5.

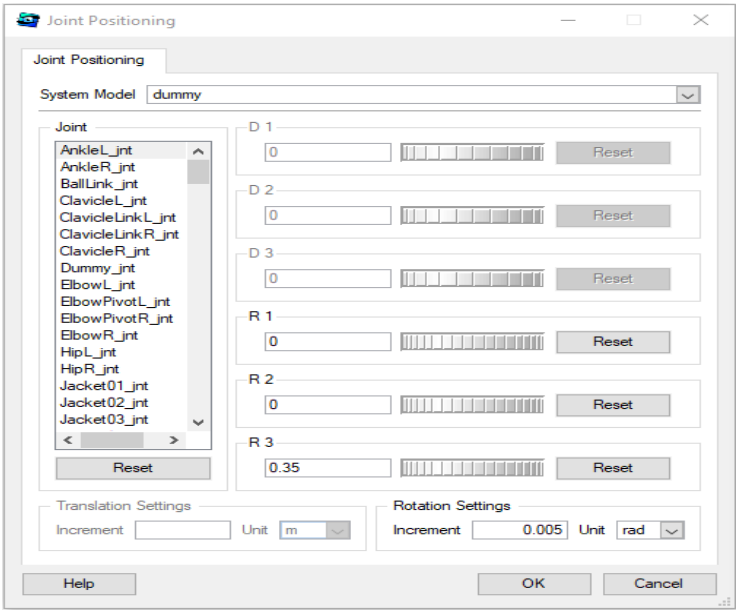

Figure 3.4. Joint Positioning Tool

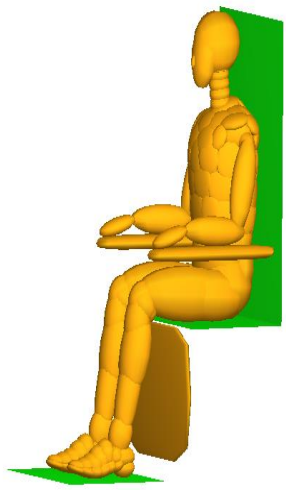

Figure 3.5. The Complete Model Representation

3.5 Restraint System Model

FE belts are created in XMADgic input deck using the belt fitting wizard, Figure 3.6. The belt width, number of element strips, element thickness is chosen accordingly. For this study two-point, three-point, four-point belt systems are created. Their points of attachment can be manually adjusted as per requirement. Surfaces in contact with the belt are assigned, desirable belt length is provided, and belt fitting is carried out. Illustration of a lap belt is shown in Figure 3.7.

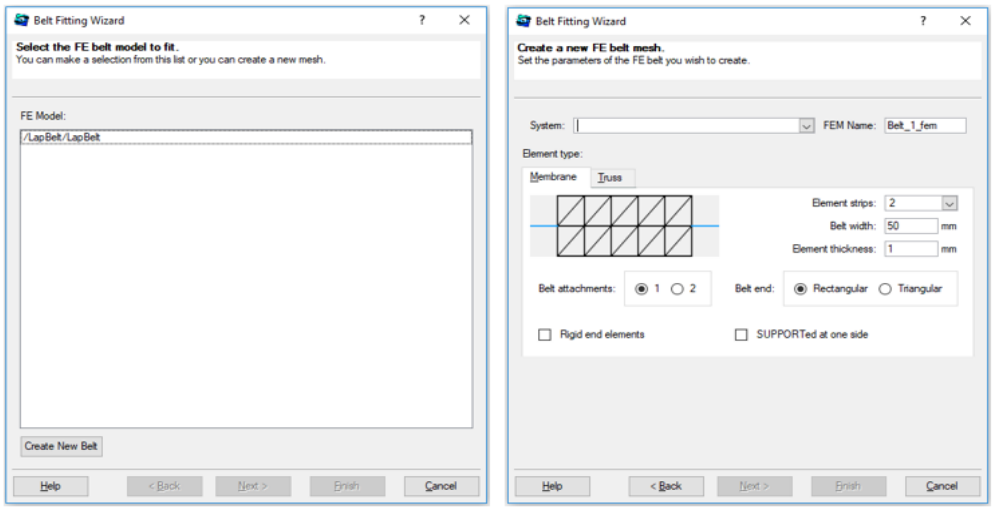

Figure 3.6 Belt fitting wizard

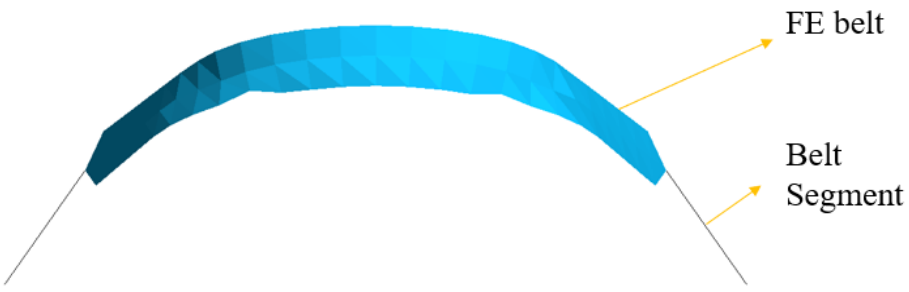

Figure 3.7.The FE Belt Model

3.4 Seat Configurations

Various seating styles have different effects on the dummy behavior. Therefore, three seating configurations have been made use of in this study. The configurations are explained in detail in forth-coming sections.

3.4.1 Configuration – I (Seat Back Angle-90º)

The basic model develops is used without any changes in this configuration. In this configuration the top seat is upright or forms a 90º angle with X-axis. In this configuration the dummy is imported and positioned upright. Representation of Seat configuration-II along with the dummy is shown in Figure 3.8.

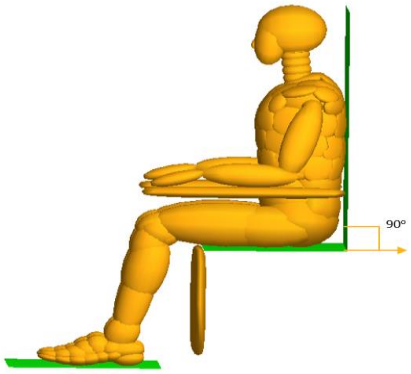

Figure 3.8 Seat Configuration-I

3.4.2 Configuration – II (Seat Back Angle-120º)

Seat back angle is increased to 120º using the joint positioning tool, Figure 3.4. After the dummy is imported and placed on the bottom seat, the entire dummy is rotated until the back of the dummy rests on the top seat. Once this is achieved the other parts are positioned individually either by translation or rotation as per requirement. Representation of Seat configuration-II is shown in Figure 3.9. Head excursion in this case is calculated from the seat reference point.

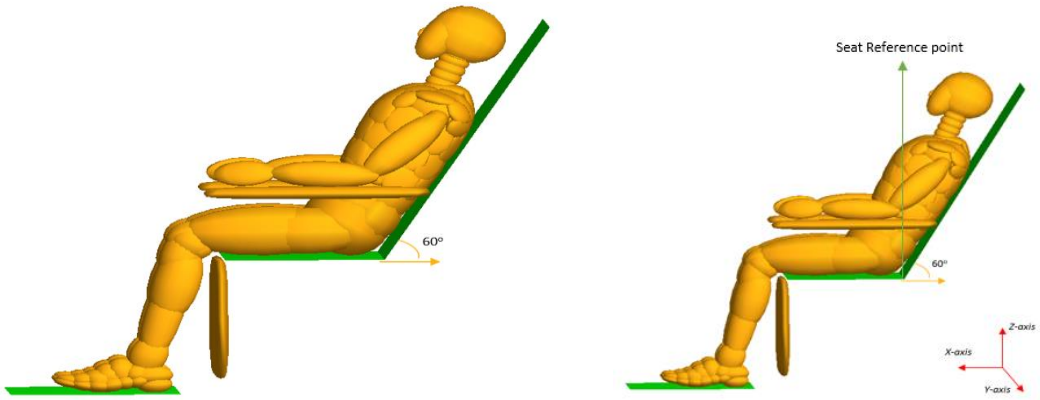

Figure 3.9 Seat Configuration-II and Seat Reference Point

3.4.3 Configuration – III (Seat Back Angle-120º, Sled Floor Angle-90º)

Seat Configuration-III shown in Figure 3.10, is obtained by applying minor modifications to configuration-II. Joint positioning tool was used to incline the sled bottom floor to 160º with respect to the X-axis and the rest remains the same. The Angle of the feet of the dummy is altered using the same tool. Head excursion in this case is calculated from the seat reference point.

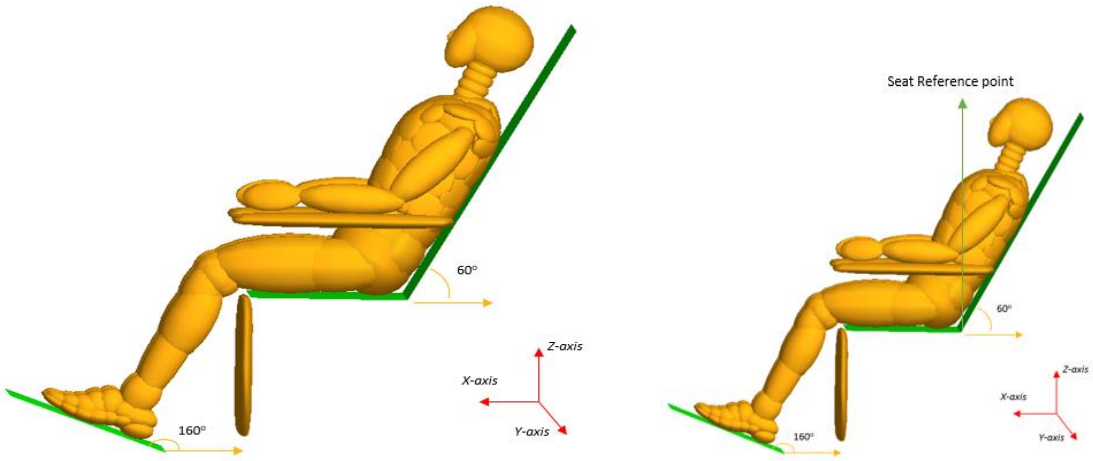

Figure 3.10 Seat Configuration-III and Seat Reference Points

3.5 Belt Configuration

Another objective of this study was to study the behavior of the dummy under various restraint system configuration. Therefore, three different configurations of seat belts were used. Two-point, Three-point, Four-point seat belts and a condition which did not employ any safety restraints was also analyzed.

3.5.1 No Belt

In this case the dummy has no restraints applied on it and moves freely during acceleration, deceleration, and Cornering. Representation of a dummy without any safety restraints is shown in Figure 3.11.

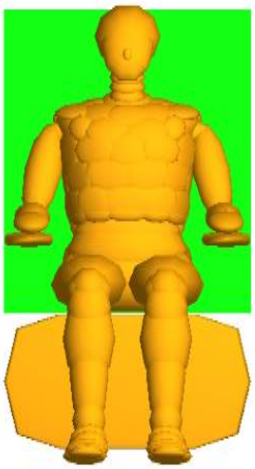

Figure 3.11 Dummy without no restraints

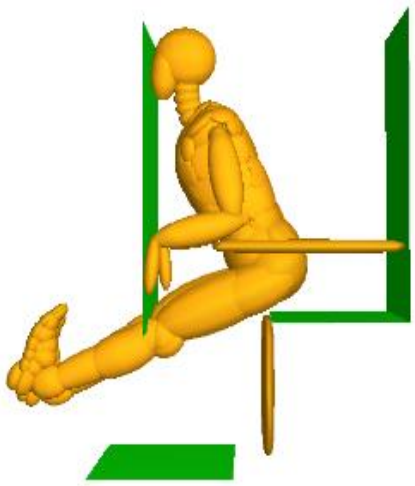

Figure 3.12 Illustration of collision with bulkhead

A bulkhead is being introduced in this no restraint system condition to evaluate the severity of injuries that might occur in the absence of a safety restraint system. Bulkhead properties have not been defined. Default stiffness of the bulkhead in the MADYMO database has been made use of for modeling. Illustration of the dummy colliding with the bulkhead is shown in Figure 3.12.

3.5.2 Two-point Seat Belt

In this configuration, the dummy has a two-point lap belt which holds the dummy in place during acceleration, deceleration and cornering. The FE lap belt, belt segments and points are created and the surfaces in contact with the belt are to be assigned until the belt fits. The point of attachment of the belt can be adjusted manually. Figure 3.13 shows the representation of a dummy restrained by a two-point belt.

3.5.3 Three-point Seat Belt

In this configuration, the dummy has a shoulder-belt in combination with a lap-belt. FE shoulder belt, belt segments and points are created in addition to the lap-belt, the surfaces in contact with the shoulder belt are assigned. The point of attachment of the belt is adjusted manually. Figure 3.14 shows the representation of a dummy restrained by a three-point belt.

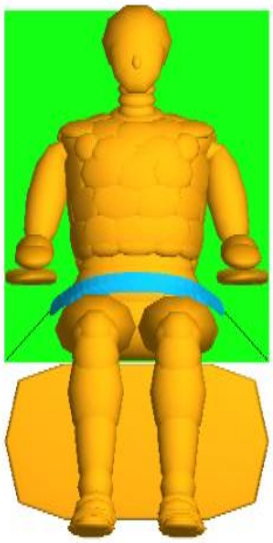

Figure 3.13. Two-point seat belt Configuration

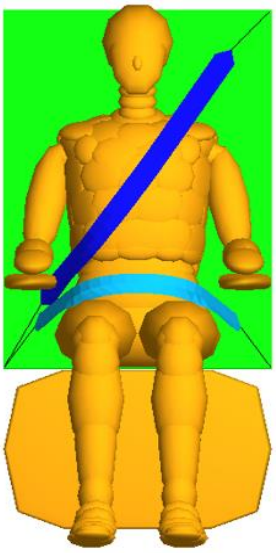

Figure 3.14 Three-point seat belt Configuration

3.5.4 Four-point Seat Belt

In this configuration, the dummy has two shoulder belts in addition to the lap belt. Two FE shoulder belts, FE lap belt, belt segments and points are created. The point of attachment of the belt is adjusted manually. In this case the lap belt and the bottom ends of the shoulder belts are attached to the bottom corner points of the top seat. And the top ends of the shoulder belts are attached to the top corners of the top seat in a crisscross manner, therefore representing a four-point belt system. The surfaces or group of surfaces in contact with the belts are assigned and belt-fitting is carried out. Figure 3.15 shows the representation of a dummy restrained by a four-point belt.

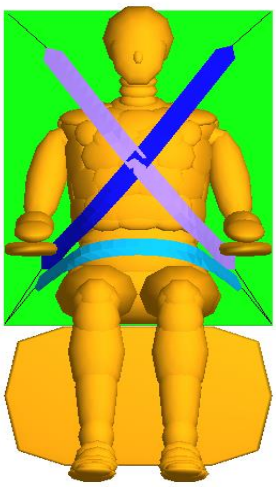

Figure 3.15 Four-Point Seat Belt Configuration

Minor changes have been made in the attachment positions of the top ends of the shoulder belts in the cornering cases. This made sure the belt functioned as intended and prevented the belt from slipping away.

CHAPTER FOUR
FINDINGS AND DISCUSSION

4.1 Findings

All tests were computational, utilizing the occupant modeling code MADYMO. Belt configurations and the no belt case were individually tested in all test conditions by applying them to each seat configuration. Acceleration, deceleration and cornering scenarios are tested separately for Test Condition-A and B. In Test Condition-C only acceleration and deceleration conditions were considered as this is a catastrophic case. In total, 96 individual cases were simulated, which included all seat and belt configurations in all test conditions. The results obtained from all the simulations were recorded, tabulated and are discussed in sections below.

4.1.1 Deceleration – Test Condition-A

Test Condition-A deals the effect of deceleration from 210mph to stand still in 15 seconds. Deceleration in this case corresponds to braking. All simulations are 500ms in duration. Since this is slower acceleration relative to the other cases, kinematic behavior does not indicate anything abnormal. For all the seating configurations, the no-belt condition results in collision with the bulk head, which indicated that even with smaller G-forces like in this case can be catastrophic without restraint systems. Various time frames of simulation of seat configurations-I, II and III in combination with various individual belt configuration are shown in tables 4.1, 4.2 and 4.3 respectively. From the simulations it can be observed that there is very slight frontal movement and minimal activation of the seat belts, irrespective of configuration. Configuration utilizing two-point lap belts show relatively higher head excursion when compared to the rest of the configurations, the minimal being the configuration utilizing the four-point belt system.

Table 4.1 *Slow* Deceleration Simulation Time frames, Seat Configuration-I (Seat back angle=90^{o})

Belt	t=0ms	t=150ms	t=300ms	t=500ms
No Belt		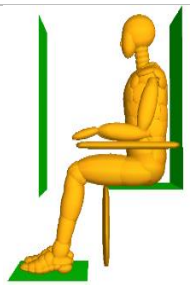	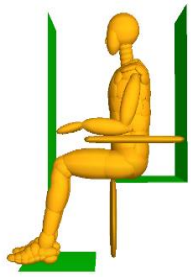	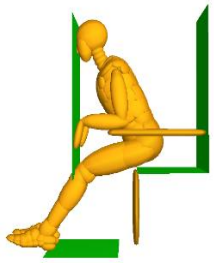
2-point Belt			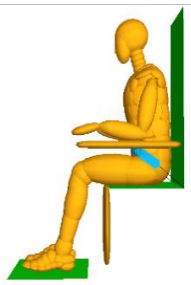	
3-point Belt		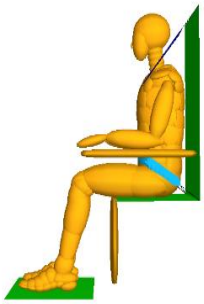		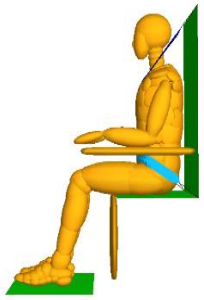
4-point Belt	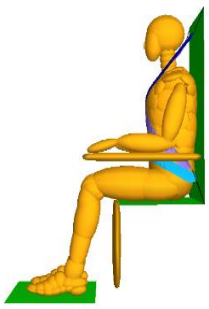	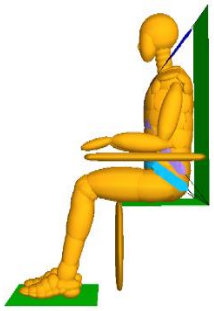	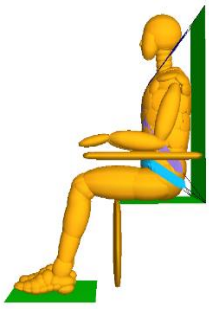	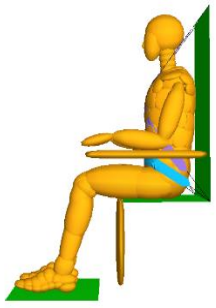

Table 4.2 *Slow* Deceleration Simulation Time frames, Seat Configuration-II (Seatback angle=120º)

Belt	t=0ms	t=150ms	t=300ms	t=500ms
No Belt		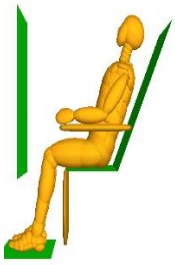	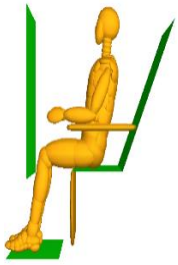	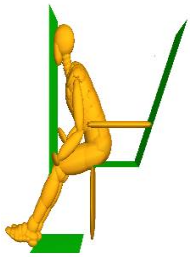
2-point Belt		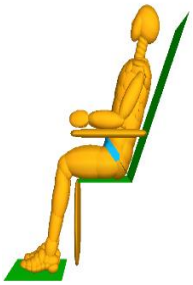		
3-point Belt		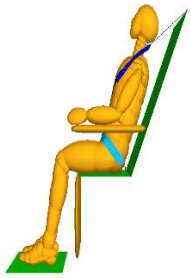	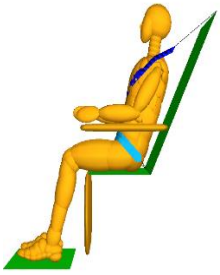	
4-point Belt			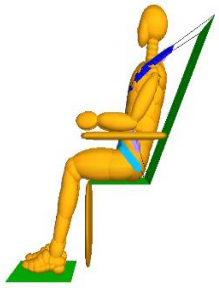	

Table 4.3 *Slow* Deceleration Simulation Time frames, Seat Configuration-III (Sled Floor angle=160º)

Belt	t=0ms	t=150ms	t=300ms	t=500ms
No Belt	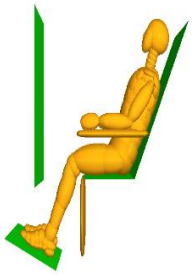	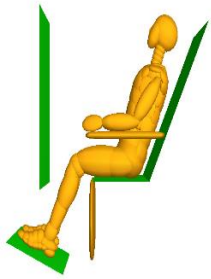	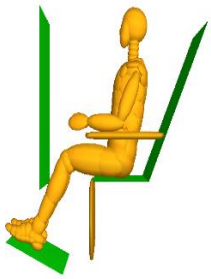	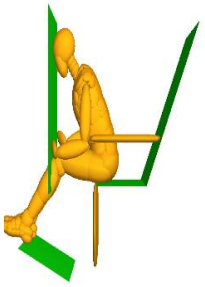
2-point Belt				
3-point Belt				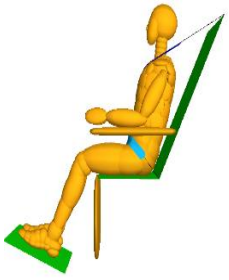
4-point Belt				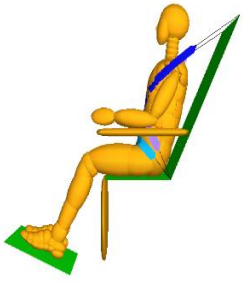

Post processor MADpost is used to record maximum values of head acceleration, head excursion, lumbar force and pelvic acceleration of the dummy in various configurations. The tabulated values are shown in Table 4.4

The color codes red and yellow indicate highest and lowest values respectively. Peach indicates the no-belt case having the highest values among the lot. Configuration-III exhibits best results among the three, and four-point configuration proves to be better in most cases except for head acceleration.

Table 4.4 Results table, **Deceleration** – Test Condition-A (Slower Acceleration)

Seat Configuration	Restraint System	Maximum Head acceleration (G)	Maximum Head Excursion(in)	Maximum Lumbar Force(kN)	Maximum Pelvic acceleration (G)	Maximum Belt forces(kN)
Configuration-I (SB angle=90°)	No belt	1920	76	6.7	525	-
	2-point	9	40.4	2.75	12.2	3.6
	3-point	9.25	14.2	0.96	16	2.35
	4-point	9.25	13.2	0.93	15	1.41
Configuration-II (SB angle=120°)	No belt	2450	70	9.25	480	-
	2-point	10	29.2	3.1	9.4	4.2
	3-point	14.6	13.2	1.7	14.8	1.6
	4-point	18.5	13	1.65	13	1.35
Configuration-III (SB angle=160°) (SF angle=90°)	No belt	2150	70	7.7	360	-
	2-point	14	29.2	3.5	12.7	3.8
	3-point	19.5	13	1.05	8.4	2.45
	4-point	16.1	12.4	1.05	8.2	1.05

SB=Seat Back, SF=Sled Floor

4.1.2 Acceleration – Test Condition-A

Time frames of simulation of seat configurations-I, II and III in combination with various individual belt configuration are shown in Tables 4.5, 4.6 and 4.7 respectively. Very subtle backward motion of the dummy is evident from the simulations, in all configurations.

Table 4.5 *Slow* Acceleration Simulation Time frames, Seat Configuration-I (Seat back angle=90°)

Belt	t=0ms	t=150ms	t=300ms	t=500ms
No Belt				
2-point Belt			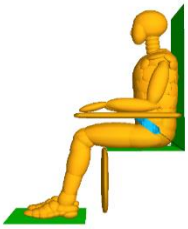	
3-point Belt				
4-point Belt				

Table 4.6 *Slow* Acceleration Simulation Time frames, Seat Configuration-II (Seatback angle=120°)

Belt	t=0ms	t=150ms	t=300ms	t=500ms
No Belt				
2-point Belt				
3-point Belt				
4-point Belt				

Table 4.7 *Slow* Acceleration Simulation Time frames, Seat Configuration-III (Sled Floor angle=160º)

Belt	t=0ms	t=150ms	t=300ms	t=500ms
No Belt				
2-point Belt				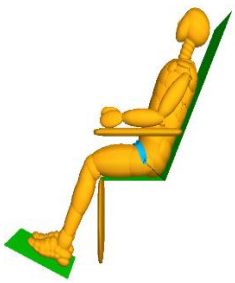
3-point Belt		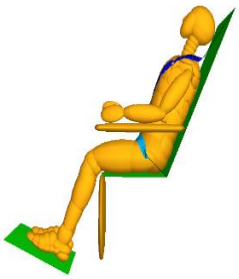	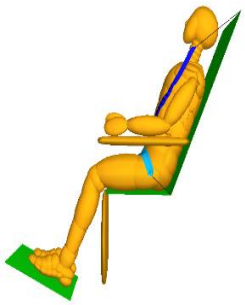	
4-point Belt		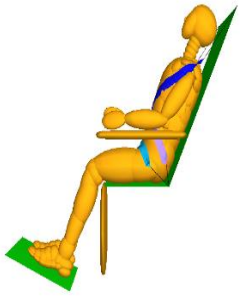		

Maximum values of head acceleration, lumbar forces, pelvic acceleration of the dummy in various seating and belt configurations are shown in Table 4.8. It is evident from the table that the injury parameter values obtained in this case are negligible and do not indicate probabilities for any potential injury. The row in peach indicates the no-belt case. Injury parameter values do not show significant variation, except for head acceleration. Seat Configuration-I seems to be the best in this case, comparing the head acceleration values.

Table 4.8. Results table, **Acceleration** – Test Condition-A (Slower Acceleration)

Seat Configuration	Belt	Maximum Head Acceleration (G)	Maximum Lumbar Forces (kN)	Maximum Pelvic Acceleration (G)	Maximum Belt Forces (kN)
Configuration-I (SB angle=90º)	No belt	1.2	0.27	1	-
	2-point	1.2	0.27	1.1	0.02
	3-point	1.2	0.27	1	0.02
	4-point	1.2	0.275	1	0.02
Configuration-II (SB angle=120º)	No belt	3.4	0.975	7.7	-
	2-point	3.3	0.9	8.2	0.01
	3-point	3.4	0.97	7.6	0.01
	4-point	3.4	0.97	8.4	0.01
Configuration-III (SB angle=160º) (SF angle=90º)	No belt	3.4	0.9	7.9	-
	2-point	3.4	0.97	8	0.01
	3-point	3.3	0.93	8.1	0.01
	4-point	3.3	0.9	8.1	0.01

SB=Seat Back, SF=Sled Floor

4.1.3 Cornering, one-mile radius of curvature – Test Condition-A

Time frames of simulation of seat configurations-I, II and III in combination with various individual belt configuration are shown in Tables 4.9, 4.10 and 4.11 respectively. Simulations indicate that the dummy collides with the armrests in all the cases. Three-point and four point belt configurations indicate probabilities of a whiplash injury and high head excursion.

Table 4.9 Cornering (210mph) Simulation Time frames, Seat Configuration-I (Seat back angle=90^{o})

Belt	t=0ms	t=50ms	t=100ms	t=150ms
No Belt				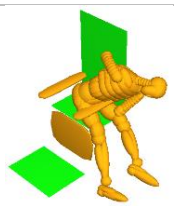
2-point Belt		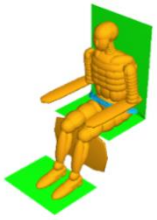		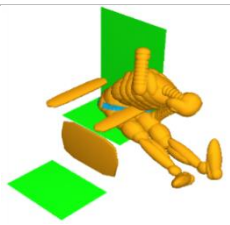
3-point Belt	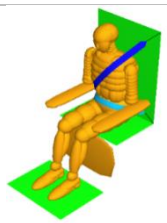	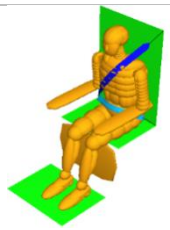	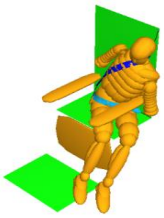	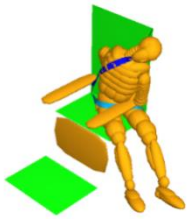
4-point Belt	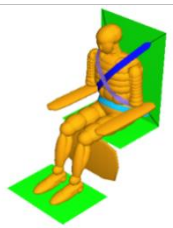	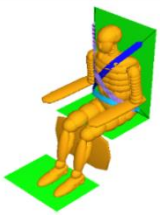	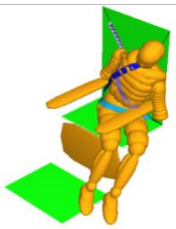	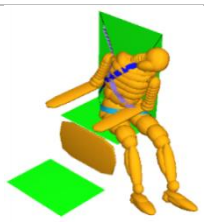

Table 4.10 Cornering (210mph) Simulation Time frames, Seat Configuration-II (Seat back angle=120^{o})

Belt	t=0ms	t=50ms	t=100ms	t=150ms
No Belt	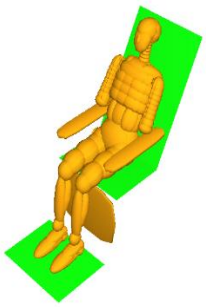	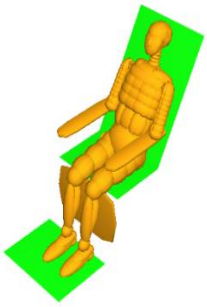		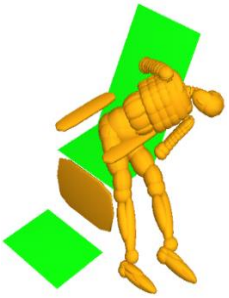
2-point Belt	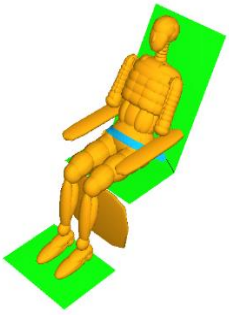	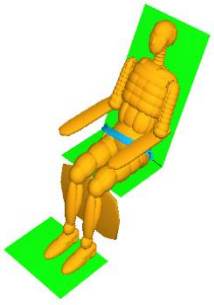		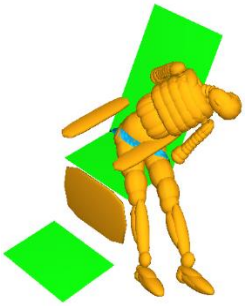
3-point Belt	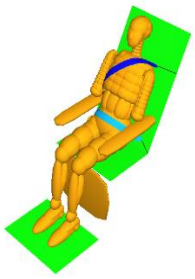	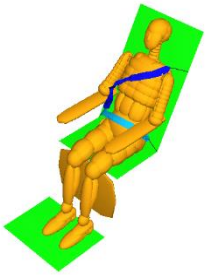	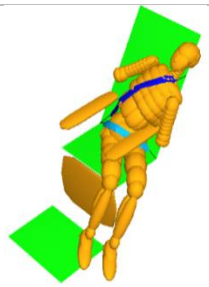	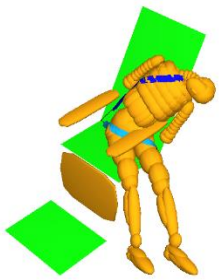
4-point Belt	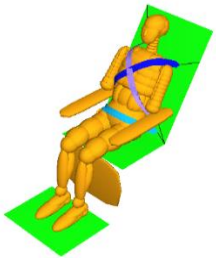	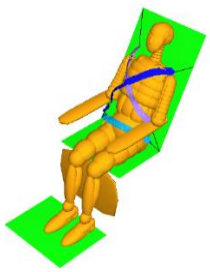	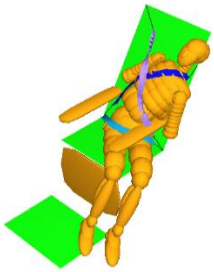	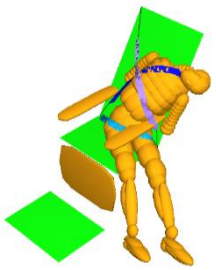

Table 4.11 Cornering (210mph) Simulation Time frames, Seat Configuration-III (Sled Floor angle=160º)

Belt	t=0ms	t=50ms	t=100ms	t=150ms
No Belt	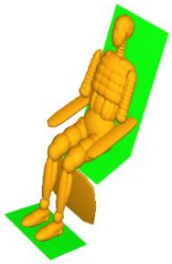	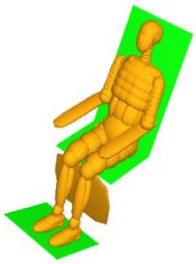		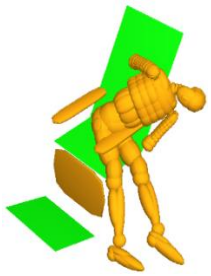
2-point Belt	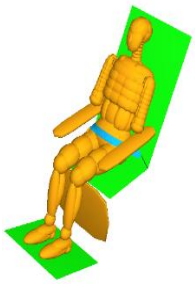	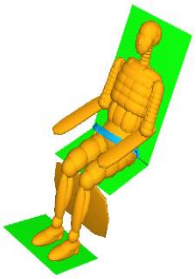	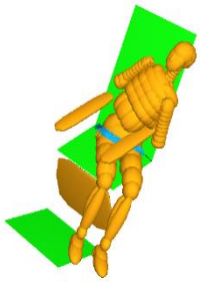	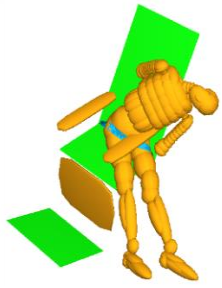
3-point Belt	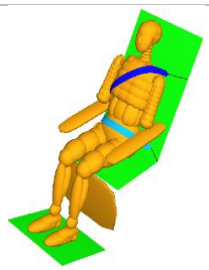	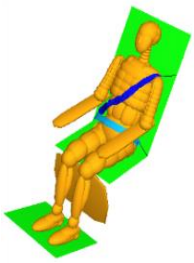	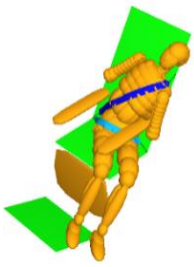	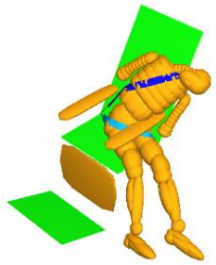
4-point Belt	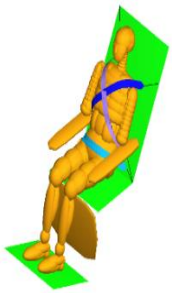	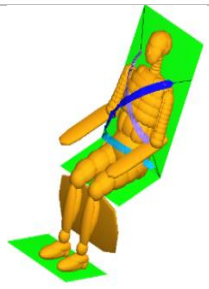	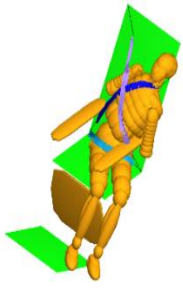	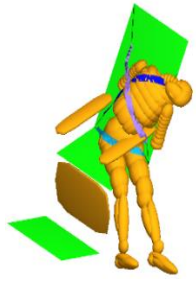

Maximum values of head acceleration, head excursion, lumbar force, pelvic acceleration, belt forces, rib deflection and viscous criterion of the EuroSID dummy in various seating and belt configurations are tabulated in Table 4.12. The color codes red and yellow indicate highest and lowest values respectively. Peach indicates the no-belt case having the highest values among the lot. Head excursion values are highest in the no-belt condition, followed by two-point configuration. Seat configuration-III exhibits relatively lower values when compared to the other configurations. Four-point belt seems to work best in all the seating configuration.

Table 4.12. Results table, **Cornering** – Test Condition-A (Slower Acceleration)

Seat Configuration	Restraint System	Maximum Head Acceleration (G)	Maximum Head Excursion (cm)	Maximum Lumbar Force (kN)	Maximum Pelvic Acceleration (G)	Maximum Belt Forces (kN)	Rib Deflection (mm)	Viscous Criterion
Configuration-I (SB angle=90º)	No belt	35	77	7.6	38	-	7.8	0.02
	2-point	43	62.2	10	30.5	5.2	6.7	0.02
	3-point	48	38.1	10	30.4	4.5	17.5	0.10
	4-point	45	35.6	6.5	30	4.5	11.5	0.06
Configuration-II (SB angle=120º)	No belt	31.5	63.5	8	26	-	6.7	0.02
	2-point	36	61	9	26	6	6.7	0.02
	3-point	48	47	8.4	25.5	3	15	0.07
	4-point	58	44.5	7	25.5	3	13	0.06
Configuration-III (SB angle=160º) (SF angle=90º)	No belt	31	75	8	26	-	6.7	0.02
	2-point	32	64.7	9	26	6.5	6.7	0.02
	3-point	31	43	7.2	25.5	4.1	6.3	0.03
	4-point	55	43	7	25	3.6	17	0.13

SB=Seat Back, SF=Sled Floor

4.1.4 Deceleration – Test Condition-B

Time frames of simulation of seat configurations-I, II and III in combination with various individual belt configuration are shown in Tables 4.13, 4.14 and 4.15 respectively. The simulations show significant frontal displacement as opposed to Test Condition-A. Head excursion is higher in the configuration utilizing two-point belt and minimal in the four-point belt system.

Table 4.13 *Fast* Deceleration Simulation Time frames, Seat Configuration-I (Seat back angle=90°)

Belt	t=0ms	t=150ms	t=300ms	t=500ms
No Belt				-
2-point Belt		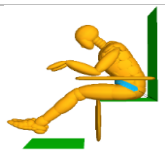	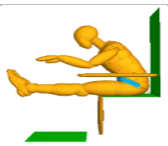	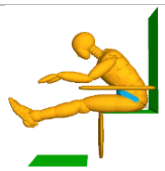
3-point Belt	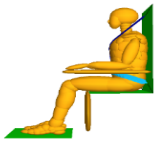	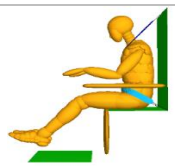	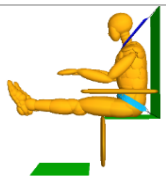	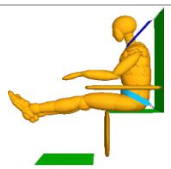
4-point Belt		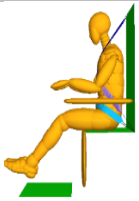		

Table 4.14 *Fast* Deceleration Simulation Time frames, Seat Configuration-II (Seatback angle=120º)

Belt	t=0ms	t=150ms	t=300ms	t=500ms
No Belt	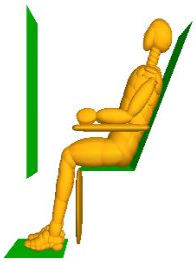	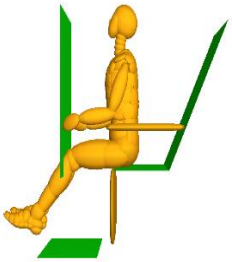	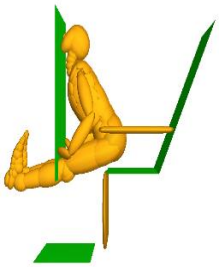	-
2-point Belt			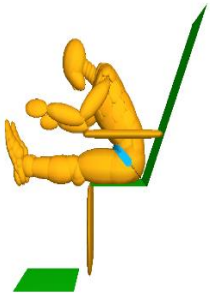	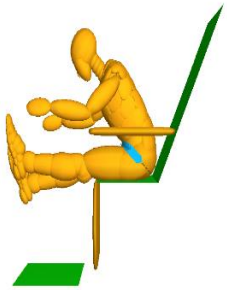
3-point Belt			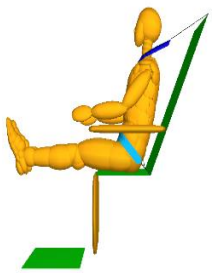	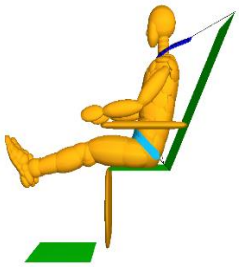
4-point Belt		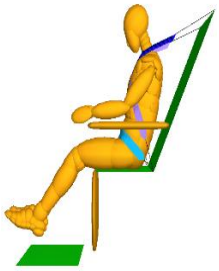	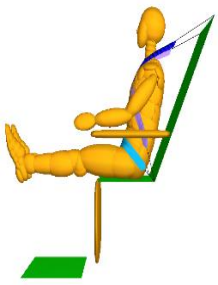	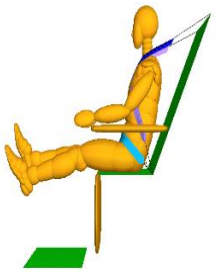

Table 4.15 *Fast* Deceleration Simulation Time frames, Seat Configuration-III (Sled Floor angle=160º)

Belt	t=0ms	t=150ms	t=300ms	t=500ms
No Belt	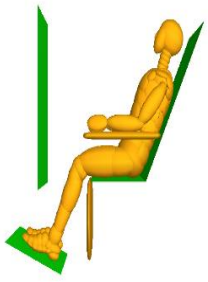	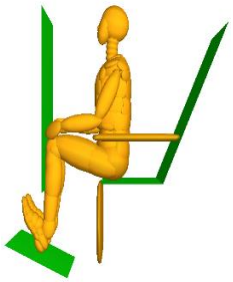		-
2-point Belt				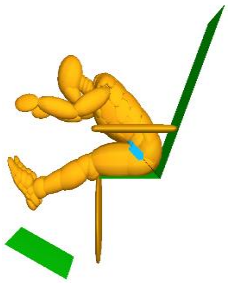
3-point Belt		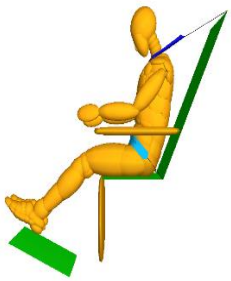	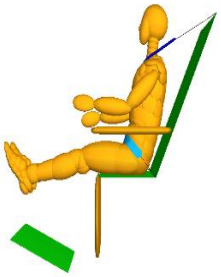	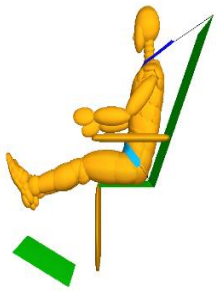
4-point Belt		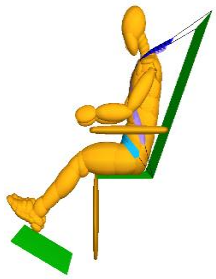	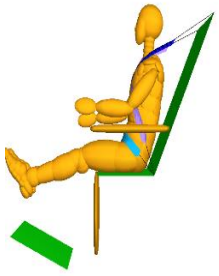	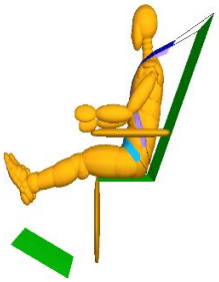

Maximum values of head acceleration, head excursion, lumbar force, pelvic acceleration and belt force in various seating and belt configurations are displayed in Table 4.16. The color codes red and yellow indicate highest and lowest values respectively and peach indicates the no-belt case. All other values except head acceleration exhibit best values when seat configuration-III is used. Pelvic acceleration values improve in seat configuration-III due to the inclination in the sled floor. Four-point belt system exhibits minimal values of all parameters except head acceleration.

Table 4.16. Results table, **Deceleration**– Test Condition-B (Faster Acceleration)

Seat Configuration	Restraint System	Maximum Head Acceleration (G)	Maximum Head Excursion (cm)	Maximum Lumbar Force (kN)	Maximum Pelvic Acceleration (G)	Maximum Belt Forces (kN)
Configuration-I (SB angle=90°)	No belt	1920	76	6.7	525	-
	2-point	9	40.4	2.75	12.2	3.6
	3-point	9.25	14.2	0.93	16	2.35
	4-point	9.25	11	0.96	15	1.41
Configuration-II (SB angle=120°)	No belt	2450	70	9.25	480	-
	2-point	10	29	3.1	9.4	4.2
	3-point	14.6	13.2	1.7	14.8	1.6
	4-point	18.5	13	1.65	13	1.35
Configuration-III (SB angle=160°) (SF angle=90°)	No belt	2150	70	7.7	360	-
	2-point	14	28	3.5	12.7	3.8
	3-point	19.5	13	1.05	8.4	2.45
	4-point	16.1	12.5	1.05	8.2	1.05

SB=Seat Back, SF=Sled Floor

4.1.5 Acceleration – Test Condition-B

Time frames of simulation of seat configurations-I, II and III in combination with various individual belt configuration are shown in Tables 4.17, 4.18 and 4.19 respectively. The dummy is pushed against the seat, while the head, shoulder, lumbar and lower back of the dummy impacts the back seat. This could indicate probabilities of injury in the absence good cushioning. Head acceleration values can be examined to confirm probabilities of injury.

Table 4.17 *Fast* Acceleration Simulation Time frames, Seat Configuration-I (Seat back angle=90°)

Belt	t=0ms	t=150ms	t=300ms	t=500ms
No Belt		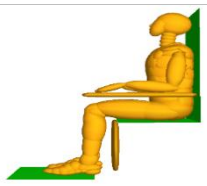	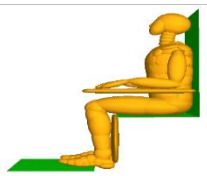	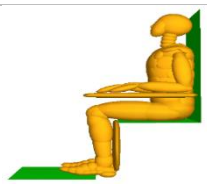
2-point Belt		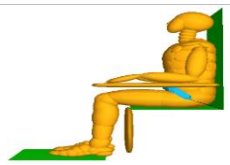	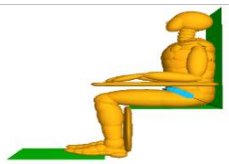	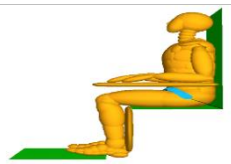
3-point Belt		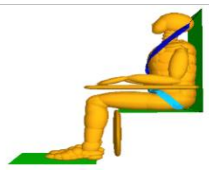	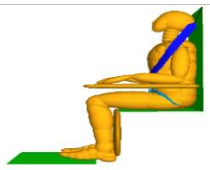	
4-point Belt	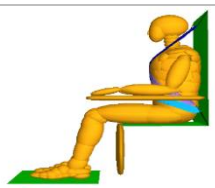	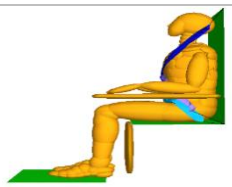	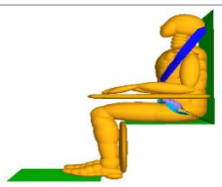	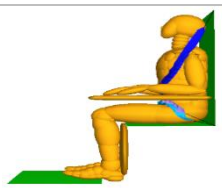

Table 4.18 *Fast* Acceleration Simulation Time frames, Seat Configuration-II (Seatback angle=120°)

Belt	t=0ms	t=150ms	t=300ms	t=500ms
No Belt		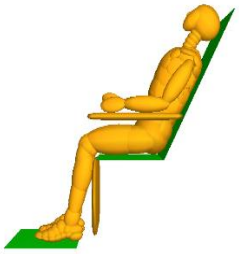	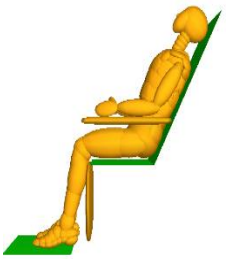	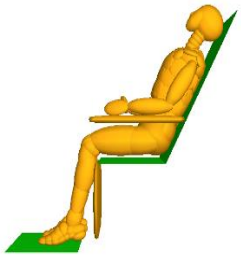
2-point Belt				
3-point Belt		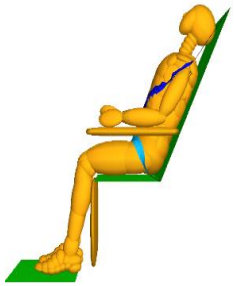		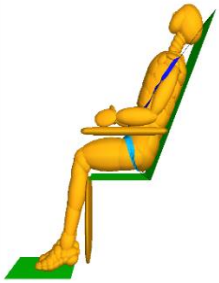
4-point Belt		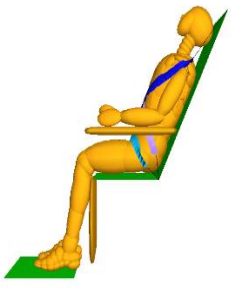		

Table 4.19 *Fast* Acceleration Simulation Time frames, Seat Configuration-III (Sled Floor angle=160º)

Belt	t=0ms	t=150ms	t=300ms	t=500ms
No Belt	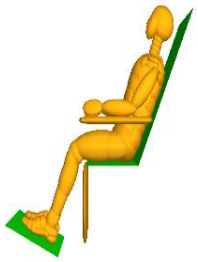	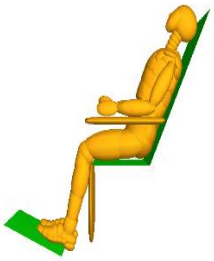	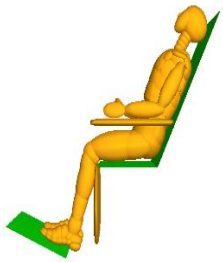	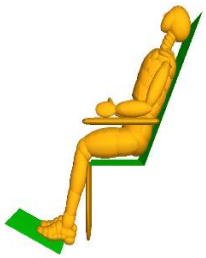
2-point Belt		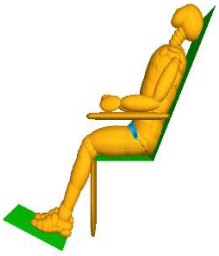	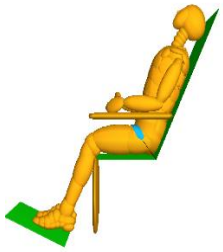	
3-point Belt		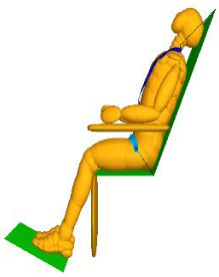		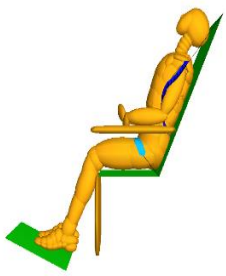
4-point Belt		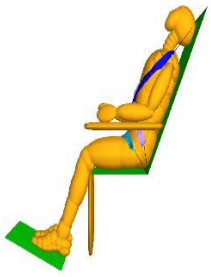		

Maximum values of head acceleration, lumbar forces, pelvic acceleration and belt forces in various seating and belt configurations are shown in Table 4.20. The values are consistent irrespective of the belt configuration used in a particular seating configuration. Seat configuration-I exhibits better head acceleration, whereas seat configuration-II and III performs better with respect to other parameters.

Table 4.20 Results table, **Acceleration**– Test Condition-B (Faster Acceleration)

Seat Configuration	Belt	Maximum Head acceleration (G)	Maximum Lumbar Forces (kN)	Maximum Pelvic Acceleration (G)	Maximum Belt forces (kN)
Configuration-I (SB angle=90º)	No belt	93	5.5	15.2	-
	2-point	93	5.5	15.2	0.02
	3-point	93	5.5	15.2	0.04
	4-point	93	5.5	15.2	0.02
Configuration-II (SB angle=120º)	No belt	132	4.56	13.5	-
	2-point	132	4.5	13.5	0.04
	3-point	132	4.5	13.5	0.05
	4-point	132	4.5	13.5	0.02
Configuration-III (SB angle=160º) (SF angle=90º)	No belt	132	4.5	13.5	-
	2-point	132	4.5	13.4	0.05
	3-point	132	4.5	13.5	0.04
	4-point	132	4.5	13.4	0.02

SB=Seat Back, SF=Sled Floor

4.1.6 Cornering, one-mile radius of curvature – Test Condition-B

Time frames of simulation of seat configurations-I, II and III in combination with various individual belt configuration are shown in Tables 4.21, 4.22 and 4.23 respectively. Simulations indicate that the dummy collides with the armrests in all the cases. It is evident from simulations that the dummy collides with the armrests in all the cases. Lateral head excursion could lead to potential injuries in case of collision with any structure that might be in the path. Three-point and four point belt configurations indicate probabilities of a whiplash injury and high head acceleration.

Table 4.21 Cornering (750mph) Simulation Time frames, Seat Configuration-I (Seat back angle=90^{o})

Belt	t=0ms	t=50ms	t=100ms	t=150ms
No Belt	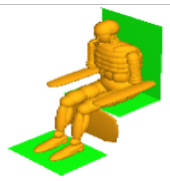	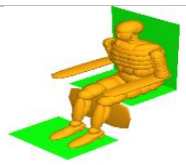	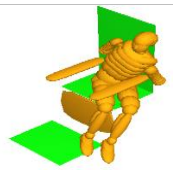	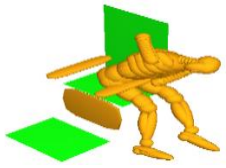
2-point Belt	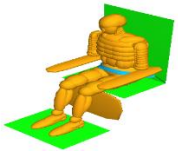	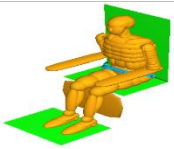	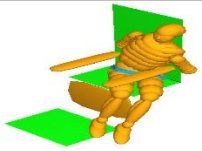	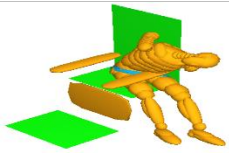
3-point Belt	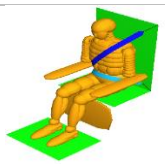	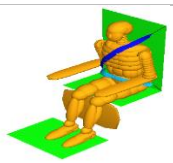	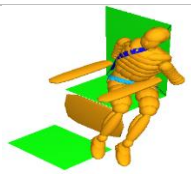	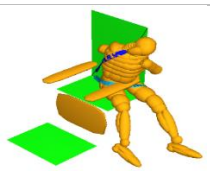
4-point Belt	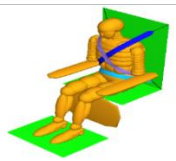	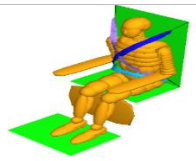	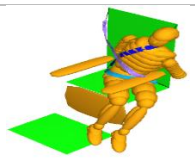	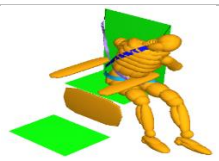

Table 4.22 Cornering (210mph) Simulation Time frames, Seat Configuration-II (Seat back angle=120^{o})

Belt	t=0ms	t=50ms	t=100ms	t=150ms
No Belt	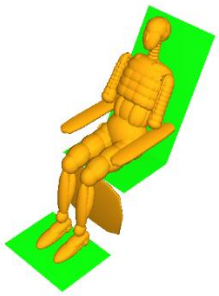	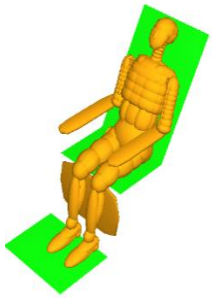		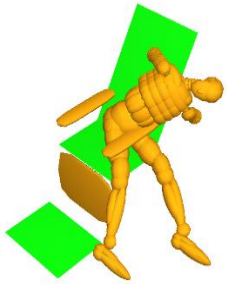
2-point Belt	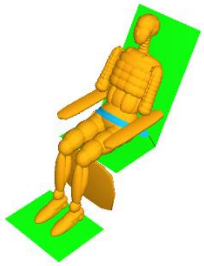	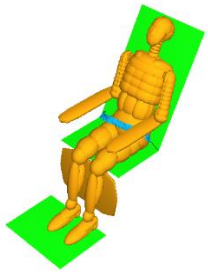	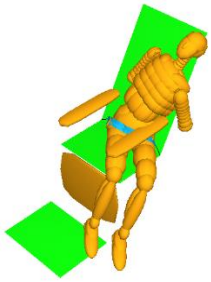	
3-point Belt	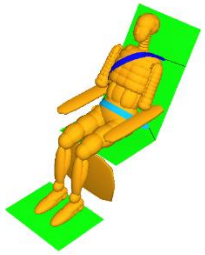	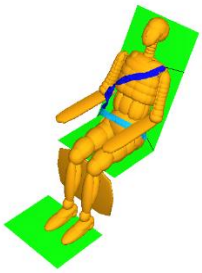	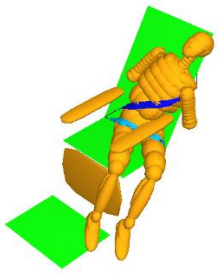	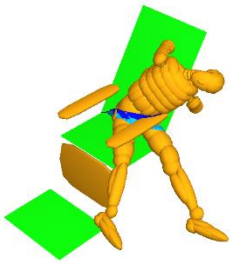
4-point Belt	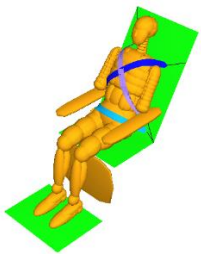	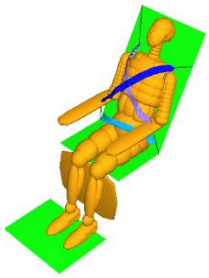	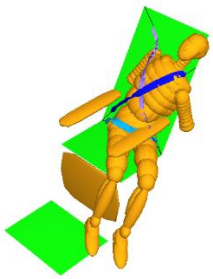	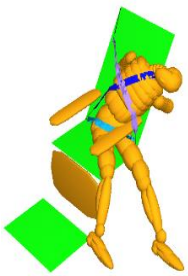

Table 4.23 Cornering (750mph) Simulation Time frames, Seat Configuration-III (Sled Floor angle=160º)

Belt	t=0ms	t=50ms	t=100ms	t=150ms
No Belt	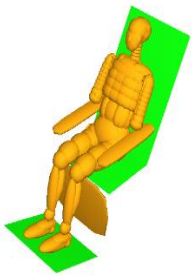	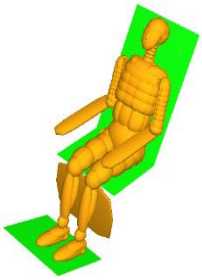	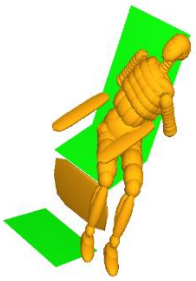	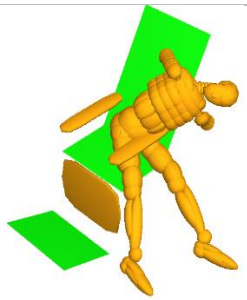
2-point Belt	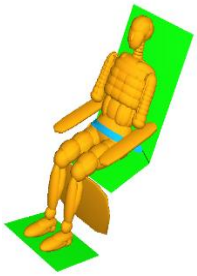	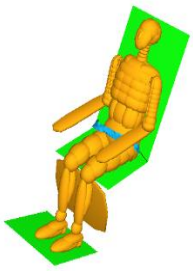	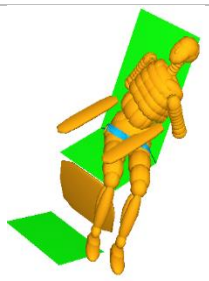	
3-point Belt	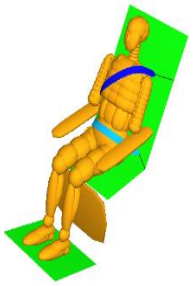	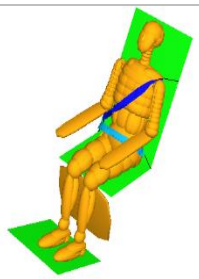	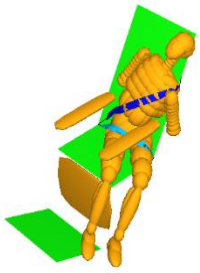	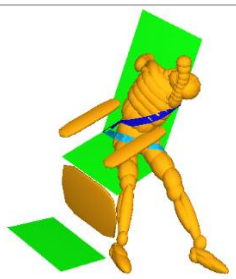
4-point Belt	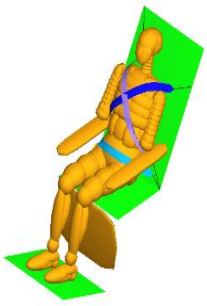	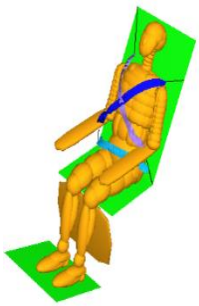	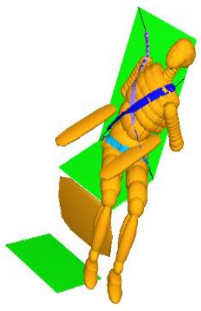	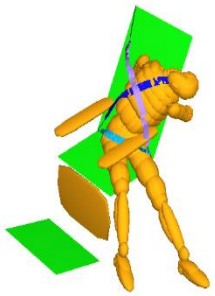

Maximum values of head acceleration, head excursion, lumbar force, pelvic acceleration, belt forces, rib deflection and viscous criterion of the EuroSID dummy in various seating and belt configurations are tabulated in Table 4.24. The color codes red and yellow indicate highest and lowest values respectively. Peach indicates the no-belt case. The table suggests two- point and three-point belt systems do not perform as per requirement. Seat configuration-III and four-point belt configuration are best suited for this case. Lateral head excursion values suggest probability of a collision with a structure in the vicinity and a potential injury.

Table 4.24 Results table, **Cornering** – Test Condition-B (Faster Acceleration)

Seat Configuration	Restraint System	Maximum Head Acceleration (G)	Maximum Head Excursion (cm)	Maximum Lumbar Force (kN)	Maximum Pelvic Acceleration (G)	Maximum Belt Forces (kN)	Rib Deflection (mm)	Viscous Criterion
Configuration-I (SB angle=90º)	No belt	38	76	8.2	30	-	6.7	0.02
	2-point	42	60	15	32	5.6	13	0.02
	3-point	40	39	11.5	28	4.8	14	0.04
	4-point	37	37	7	28	3.8	12	0.09
Configuration-II (SB angle=120º)	No belt	19	70	7	26	-	5.3	0.01
	2-point	25	66	8	26	6.3	5.3	0.01
	3-point	40	60	10.5	33	4.3	5.2	0.02
	4-point	39	44	7	25	3.1	5.2	0.01
Configuration-III (SB angle=160º) (SF angle=90º)	No belt	20	70	7	26	-	5.3	0.01
	2-point	25	64	9	26	3.4	5.2	0.02
	3-point	40	42	6	25	4	5	0.03
	4-point	38	43	7.5	25	3	5	0.01

SB=Seat Back, SF=Sled Floor

4.1.7 Deceleration – Test Condition-C

Time frames of simulation of seat configurations-I, II and III in combination with various individual belt configuration are shown in Tables 4.25, 4.26 and 4.27 respectively. The simulations confirm chances of a whiplash injury in almost all cases. Two-point belt configuration condition indicates probable collision of the dummy's head with its own knee. It is evident from the simulations that any seating or belt configuration considered in this study does not make it any safer for the occupant.

Table 4.25 *Severe Case* Deceleration Simulation Time frames, Seat Configuration-I (Seat back angle=90^{o})

Belt	t=0ms	t=250ms	t=500ms	t=1000ms
No Belt		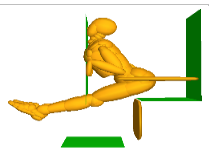	-	-
2-point Belt		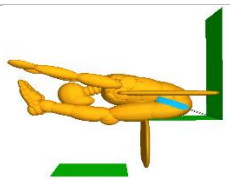	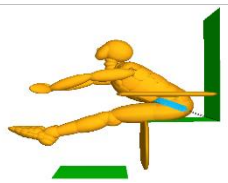	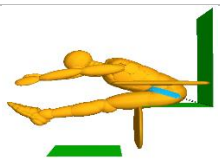
3-point Belt		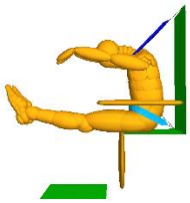	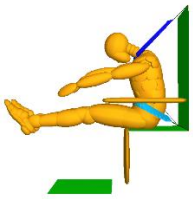	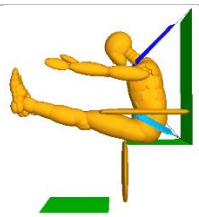
4-point Belt		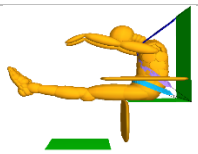	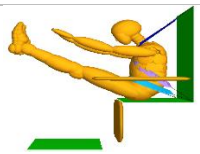	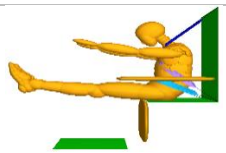

Table 4.26 *Severe Case* Deceleration Simulation Time frames, Seat Configuration-II (Seatback angle=120°)

Belt	t=0ms	t=250ms	t=500ms	t=1000ms
No Belt		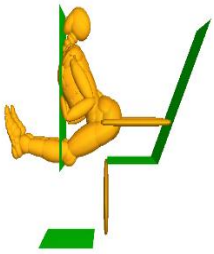	-	-
2-point Belt		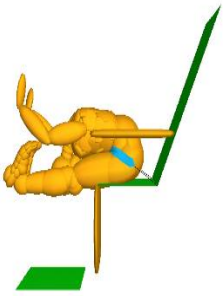		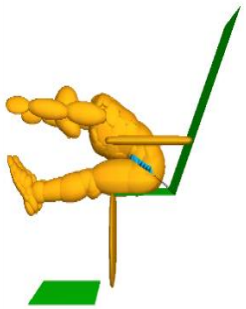
3-point Belt		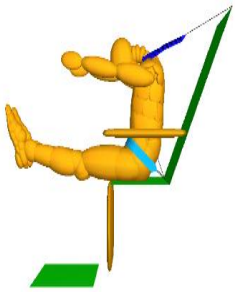	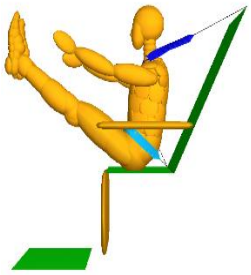	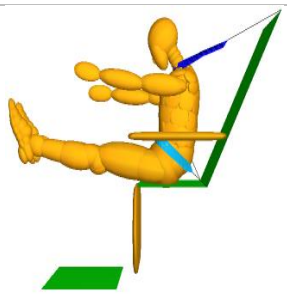
4-point Belt		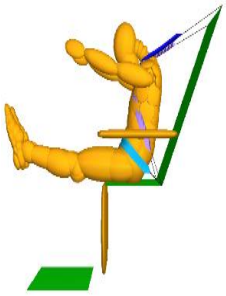	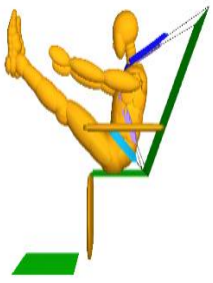	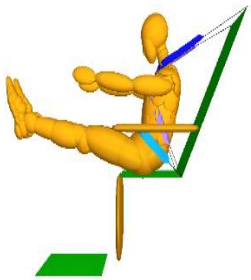

Table 4.27 *Severe Case* Deceleration Simulation Time frames, Seat Configuration-III (Sled Floor angle=160°)

Belt	t=0ms	t=250ms	t=500ms	t=1000ms
No Belt			-	-
2-point Belt		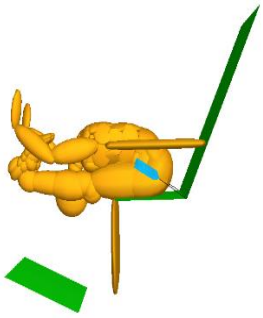	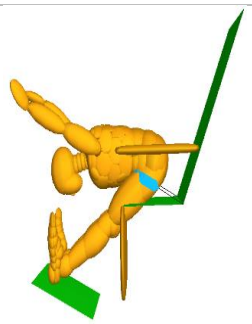	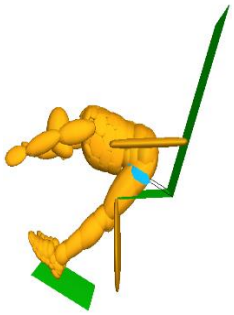
3-point Belt		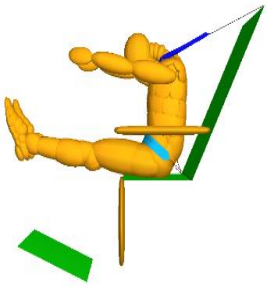	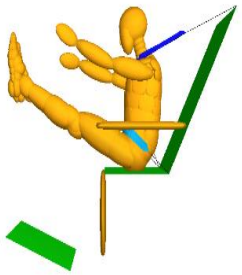	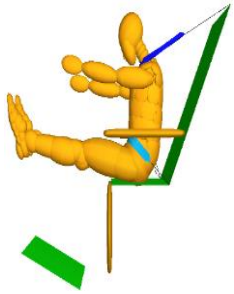
4-point Belt		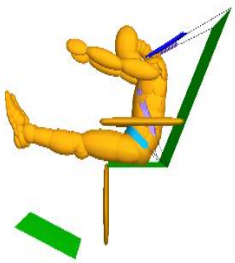	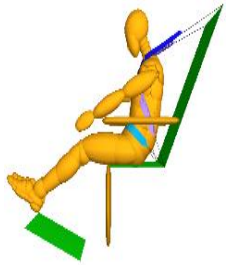	

Maximum values of head acceleration, head excursion, lumbar force, pelvic acceleration and belt force in various seating and belt configurations are displayed in Table 4.28. The color codes red and yellow indicate highest and lowest values respectively and peach indicates the no-belt case. All other values except head acceleration exhibit best values when seat configuration-III is used. This being an extreme case probability of injury is very high. It can be noted that the value of head excursion is much higher than that of the no belt condition, which indicates that the head of the dummy crossed the distance at which the bulkhead was placed. Four-point configuration exhibits minimal values in most of the cases.

Table 4.28 Results table, **Deceleration**– Test Condition-C (Most Severe Case)

Seat Configuration	Restraint System	Maximum Head Acceleration (G)	Maximum Head Excursion (cm)	Maximum Lumbar Force (kN)	Maximum Pelvic Acceleration (G)	Maximum Belt Forces (kN)
Configuration-I (SB angle=90°)	No belt	2700	55	10	830	-
	2-point	41	65	14	41.5	15
	3-point	42	33	3.7	41	11.5
	4-point	41	25	3	42	5
Configuration-II (SB angle=120°)	No belt	2720	67	10	830	-
	2-point	41	70	14	41	14.8
	3-point	42	29	3.7	41	12
	4-point	42	5.3	2.5	39	10
Configuration-III (SB angle=160°) (SF angle=90°)	No belt	4500	67	7.5	95	-
	2-point	48	72	14	41.5	14.7
	3-point	44	25.6	3	44.5	13
	4-point	42	22.6	2	43	10.5

SB=Seat Back, SF=Sled Floor

4.1.8 Acceleration – Test Condition-C

Time frames of simulation of seat configurations-I, II and III in combination with various individual belt configuration are shown in Tables 4.29, 4.30 and 4.31 respectively. The head, shoulder, lumbar and lower back of the dummy impacts the back seat. This indicates probabilities of high head acceleration and skull fracture depending on the stiffness of the seat. Injury parameters must be examined to confirm probabilities of injury.

Table 4.29 *Severe Case* Acceleration Simulation Time frames, Seat Configuration-I (Seat back angle=90°)

Belt	t=0ms	t=150ms	t=300ms	t=500ms
No Belt		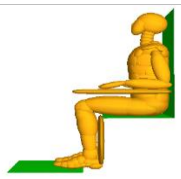	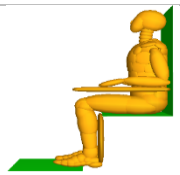	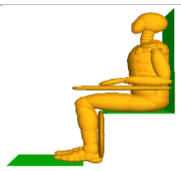
2-point Belt		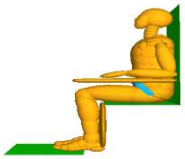		
3-point Belt		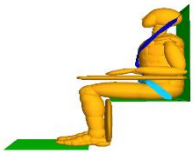	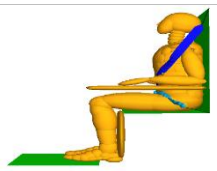	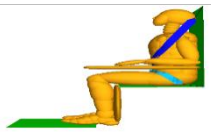
4-point Belt		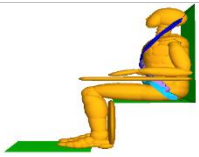	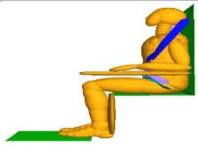	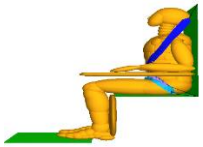

Table 4.30 *Severe Case* Acceleration Simulation Time frames, Seat Configuration-II (Seatback angle=120°)

Belt	t=0ms	t=150ms	t=300ms	t=500ms
No Belt	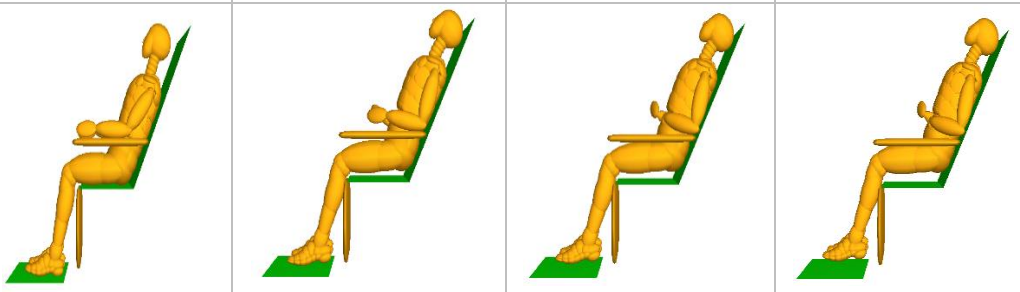			
2-point Belt	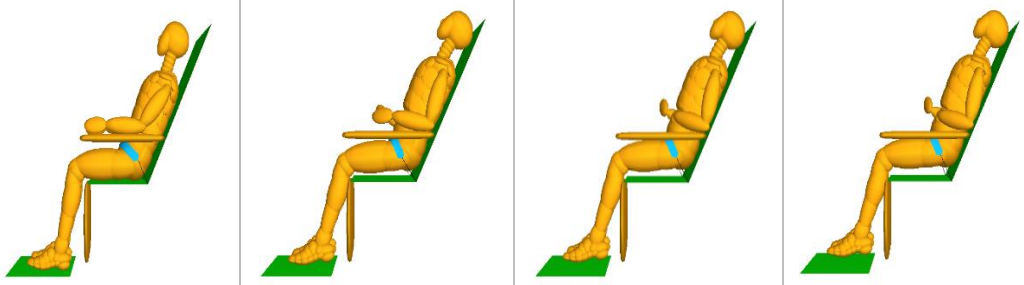			
3-point Belt	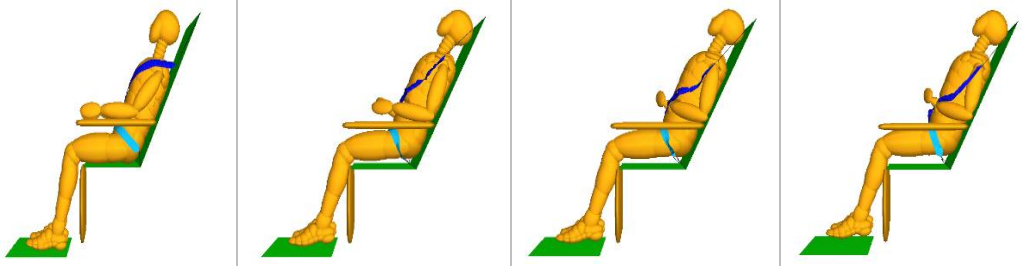			
4-point Belt	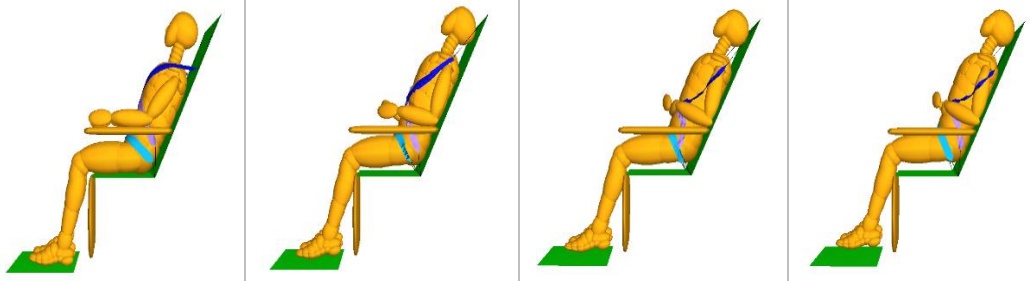			

Table 4.31 *Severe Case* Acceleration Simulation Time frames, Seat Configuration-III (Sled Floor angle=160°)

Belt	t=0ms	t=150ms	t=300ms	t=500ms
No Belt		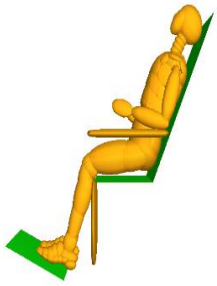	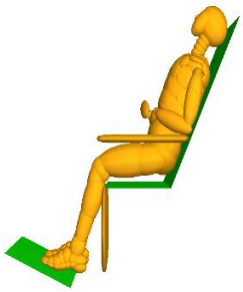	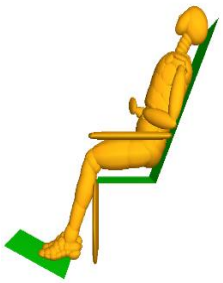
2-point Belt			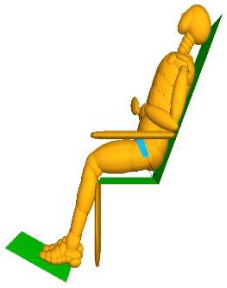	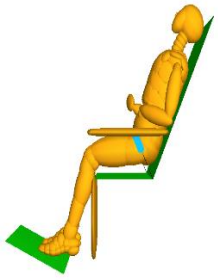
3-point Belt		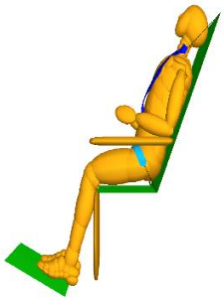		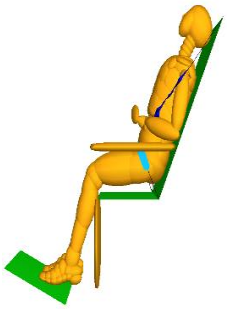
4-point Belt		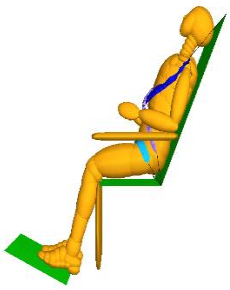	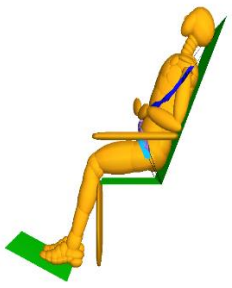	

Maximum values of head acceleration, lumbar forces, pelvic acceleration and belt forces in various seating and belt configurations are shown in Table 4.32. The values of head acceleration indicate high probabilities of skull fracture [22]. Variation of values with respect to belt configuration remains minimal. Seat configuration-I exhibits better results in case of head acceleration, whereas seat configuration-II and III seem to be better when looked into other parameters.

Table 4.32 Results table, **Acceleration**– Test Condition-C (Most Severe Case)

Seat Configuration	Belt	Maximum Head acceleration (G)	Maximum Lumbar Forces (kN)	Maximum Pelvic Acceleration (G)	Maximum Belt forces (kN)
Configuration-I (SB angle=90°)	No belt	245	9.25	27.1	-
	2-point	241	9.25	27	0.02
	3-point	241	9.3	27	0.03
	4-point	242	9.2	27.1	0.03
Configuration-II (SB angle=120°)	No belt	255	6.7	19.9	-
	2-point	255.9	6.6	19.8	0.6
	3-point	255.9	6.5	19.6	0.6
	4-point	255	6.7	19.9	0.6
Configuration-III (SB angle=160°) (SF angle=90°)	No belt	247	6.8	19.6	-
	2-point	246.9	6.5	19.5	0.45
	3-point	247	6.6	19.5	0.47
	4-point	247	6.5	19.5	0.5

SB=Seat Back, SF=Sled Floor

4.2 Discussion

It is evident from the values of high head acceleration the probabilities of injury occurring is high. There is an estimated a 5% risk of skull fractures for a peak acceleration of 180G and a 40% risk of fractures for 250G. Therefore, in case of deceleration in Test Condition-B and C the probabilities of head injury are high. Head acceleration values were found to be minimal for seat configuration-I.

In the deceleration scenarios the recorded head excursion is frontal, whereas in case of cornering the head excursion is lateral. Head excursion values for cornering cases are consistently high for all considered test conditions. It has a 40-50% dip in certain configuration-III, four-point belt cases. High values of head excursion in the cornering cases indicates high probability of head impact on the structures in the range of it.

High pelvis-acceleration indicates high probability of pelvis injury. The values are consistently high in almost all cases and considerably high in cornering scenarios. There is a 10-30% dip in pelvis acceleration while tested with seat configuration-III.

Lumbar forces and belt forces are not extremely high. Yet again least values of lumbar forces are seen when tested with seat configuration-III in combination with a four-point seat belt.

Examining the kinematics makes it clear that Test Condition-C is way more intense and catastrophic when compared to test condition A and B. The side armrest plays an important role in retaining the dummy on the seat in the cornering scenarios, but also increases probability of potential injury.

All the measured parameters and the kinematics clearly indicates that seat configuration-III along with the four point-restraint system yields best results.

CHAPTER FIVE

DESIGN OF CHARTS / KRIGING MODEL

5.1 Kriging Model

A response surface data generated by interpolation of computational results obtained is utilized in the design of charts. Initial design points are selected, from which the performance oriented data is extracted using MADYMO. A set of design parameters from each simulation are utilized to generate a set of results. These are then utilized to build the kriging model. Optimizing results and developing a prediction model to reduce the number of simulations and also arriving at the optimal design configuration forms the major objective of this process.

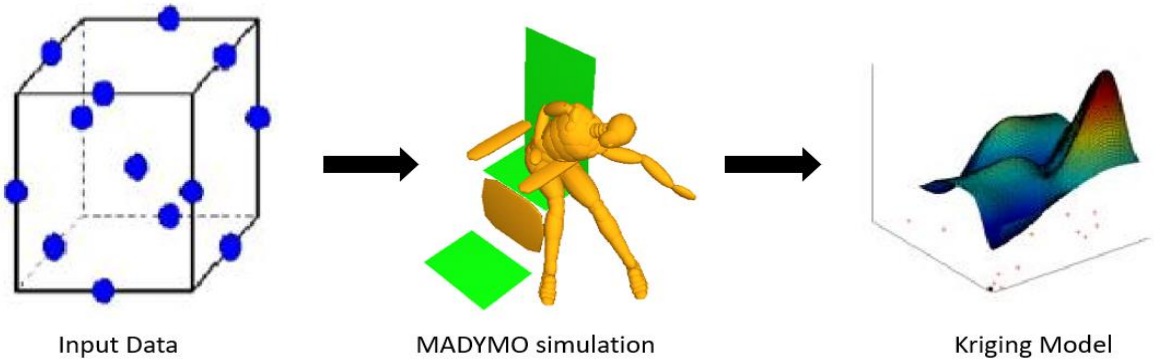

Figure 5.1 Flowchart representation of the Kriging process

Kriging model is built using the multi-objective optimization method to interpolate the given set of sample points to a model approximately. A Kriging model to estimate the unknown function y (x) can be expressed as [20,21]

$$Y(x) = \mu + Z(x) \tag{5.1}$$

'x' is m-dimensional vector, Y(x) is the unknown function, 'μ' is the constant global model and Z(x) is the realization of a Gaussian stochastic process which represents the local deviation from the global model. The correlation for the Z(x) matrix can be given by [20, 21]

$$\text{Corr}[Z(x_i, x_j)] = \sigma^2 \; d(x_i, x_j) \tag{5.2}$$

distance between the two sample points x_i and x_j can be expressed as follows [20, 21]

$$d(x_i, x_j) = -\left[\exp \; \sum_{k=1}^{m} \Theta_k |x_k^i - x_k^j|^2 \right] \tag{5.3}$$

Θ_k is the kth element of the correlation vector and term inside the exponential gives the between two sample point x_i, x_j. Considering 'n' sample points the like hood function of model parameters is be given [20, 21] by:

$$Likelihood = -\frac{n}{2} ln(2\pi) - \frac{n}{2} ln\, \sigma^2 - \frac{1}{2} ln \left| R \right| - \frac{1}{2\sigma^2} (y - A\mu)^T R^{-1} (y - A\mu) \tag{5.4}$$

'y' is the column vector response, 'A' denotes the m dimensional unit vector, 'R' denotes the n×m matrix whose (i, j) entry is Corr[Z(x_i , x_j)]. The parameters μ and σ^2 can be defined as [20, 21]

$$\mu = [A^t R^{-1} Y]^{-1} A^t R^{-1} y \tag{5.5}$$

σ^2 can be estimated as:

$$\sigma^2 = \frac{(y - A\mu)^t R^{-1} (y - A\mu)}{n} \tag{5.6}$$

Using Equations (5.5) and (5.6), the likelihood function can be transformed and maximized. Therefore, correlation matrix R can be calculated. The Kriging predictive model is given by

$$y(x^*) = \mu + r^t(x^*)R^{-1}(y\text{-}A\mu) \quad (5.7)$$

which is used to predict the model response at a different set of input values [20, 21].

5.2 Input and Output Parameters

A set of input parameters are identified and the results corresponding to them, obtained from MADYMO simulations are input into the kriging model. The generated surface plot helps in understanding how the results are varied for a given set of design variables. A surface plot consists of three axes; i.e. x-axis, y-axis and z-axis. In this case x-axis and y-axis remain unchanged. X-axis represents the belt configuration and y-axis represents the Seating configurations. Z-axis represents the results obtained from MADYMO or the output Data; i.e. head excursion, lumbar forces, pelvic acceleration, and belt loads for deceleration condition. Pelvic acceleration, rib deflection, viscous criterion in case of cornering. Nine data points are considered, therefore nine values of results obtained from various conditions corresponding to input parameters are entered into the system. The input and output parameters considered are summarized in Table 5.1.

Table 5.1 Input and Output Parameters

Input parameters	**Output parameters (Fast Deceleration)**	**Output parameters (Cornering-750mph)**
Belt Configurations 1. Two-point 2. Three-point 3. Four-point	1. Head Excursion 2. Lumbar Forces 3. Pelvic Acceleration 4. Belt Loads	1. Pelvis Acceleration 2. Rib Deflection 3. Viscous Criterion
Seat Configurations 1. Configuration-1 2. Configuration-2 3. Configuration-3		

5.3 Generated Surface Plots for Deceleration, Test Condition-B (Fast Deceleration)

Surface plots are generated for deceleration condition of Test Condition-B, which deals with the velocity at which the Hyperloop is expected to operate. Therefore, studying the variation of these results would be extremely beneficial in selection of design criteria, safety restraint systems and seat configuration.

5.3.1 Belt Loads

The surface plot showing the variation of belt loads (F_B) with respect to belt and seat configuration is shown in the Figure 5.2. It is observed from the plot that values of belt load for two-point belt system, irrespective of the seating configuration is much higher than that of other configurations. The values of belt loads exhibited by the three-point configuration is significantly higher than values of four-point belt configuration. Considering just the four-point belt configuration, the value obtained from seat configuration-III is the least.

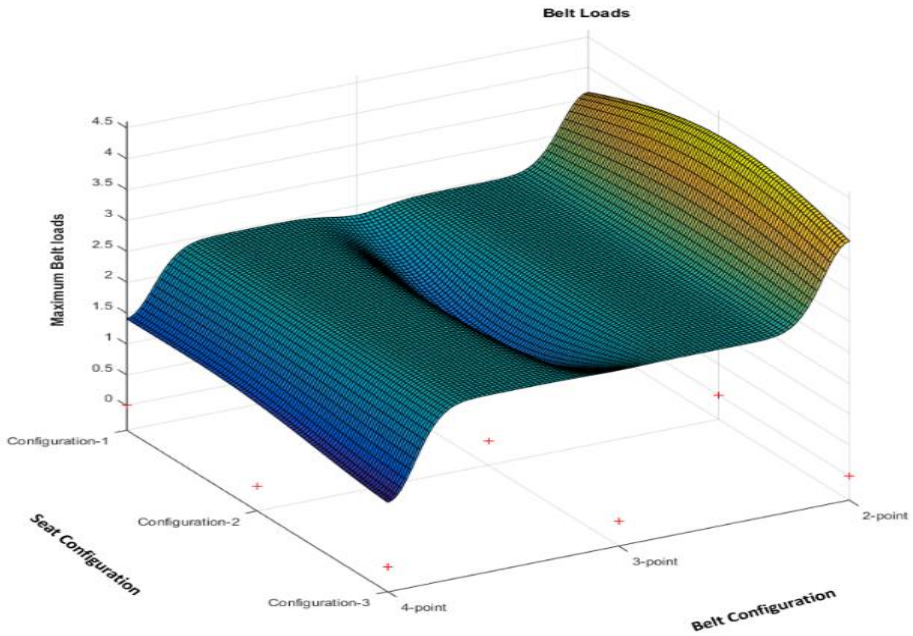

Figure 5.2. Surface Plot Showing Belt Loads

5.3.1 Head excursion

Head excursion (Δ_H) variation with respect to belt and seat configurations is shown in Figure 5.3. Examining the plot shows that the value of head excursion is the highest for seat configuration-I when combined with a two-point belt system. Values corresponding to three-point and four-point configurations are much lower and does not show a significant difference. The least value corresponds to seat configuration-III and four-point belt system.

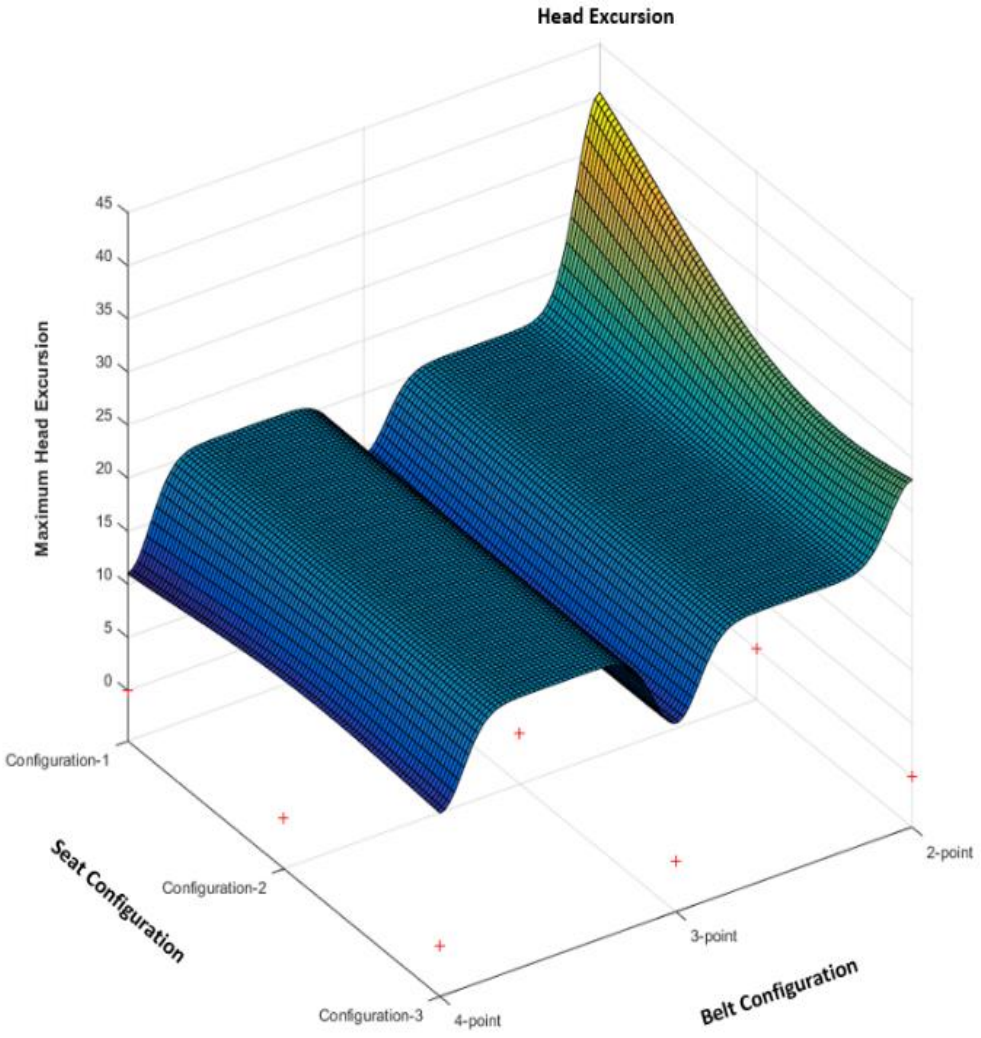

Figure 5.3. Surface Plot Showing Head Excursion

5.3.3 Lumbar Forces

Figure 5.4 shows the surface plot, showing the variation of lumbar Forces (F_L) with respect to Seat and belt configuration. It is evident from the plot that, values corresponding to two-point belt system is highest. Values corresponding to three-point and four-point belt systems do not vary considerably, but the least value is obtained from four-point system and Seat configuration-III

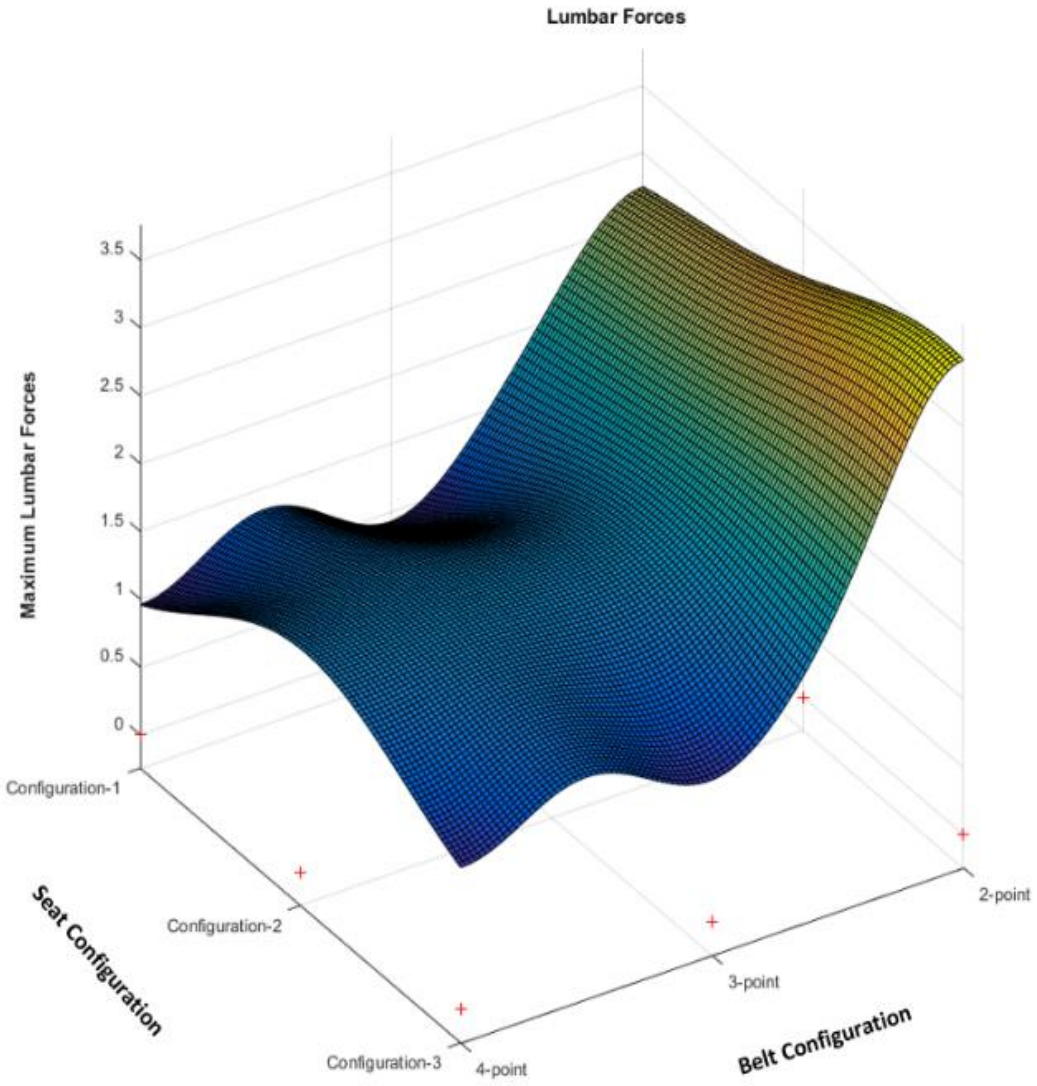

Figure 5.4 Surface Plot Showing Lumbar forces

5.3.3 Pelvic Acceleration

Variation of pelvic acceleration (A_P) with respect to belt and seat configurations is shown in Figure 5.5. Pelvic acceleration corresponding to the two-point belt configuration are on the lower side. Values obtained from three-point belt system corresponding to seat configuration-I is the highest and gradual decrease can be noticed as it approaches seat configuration-III. Least value of pelvic acceleration is the one corresponding to seat configuration-III and four-point belt system.

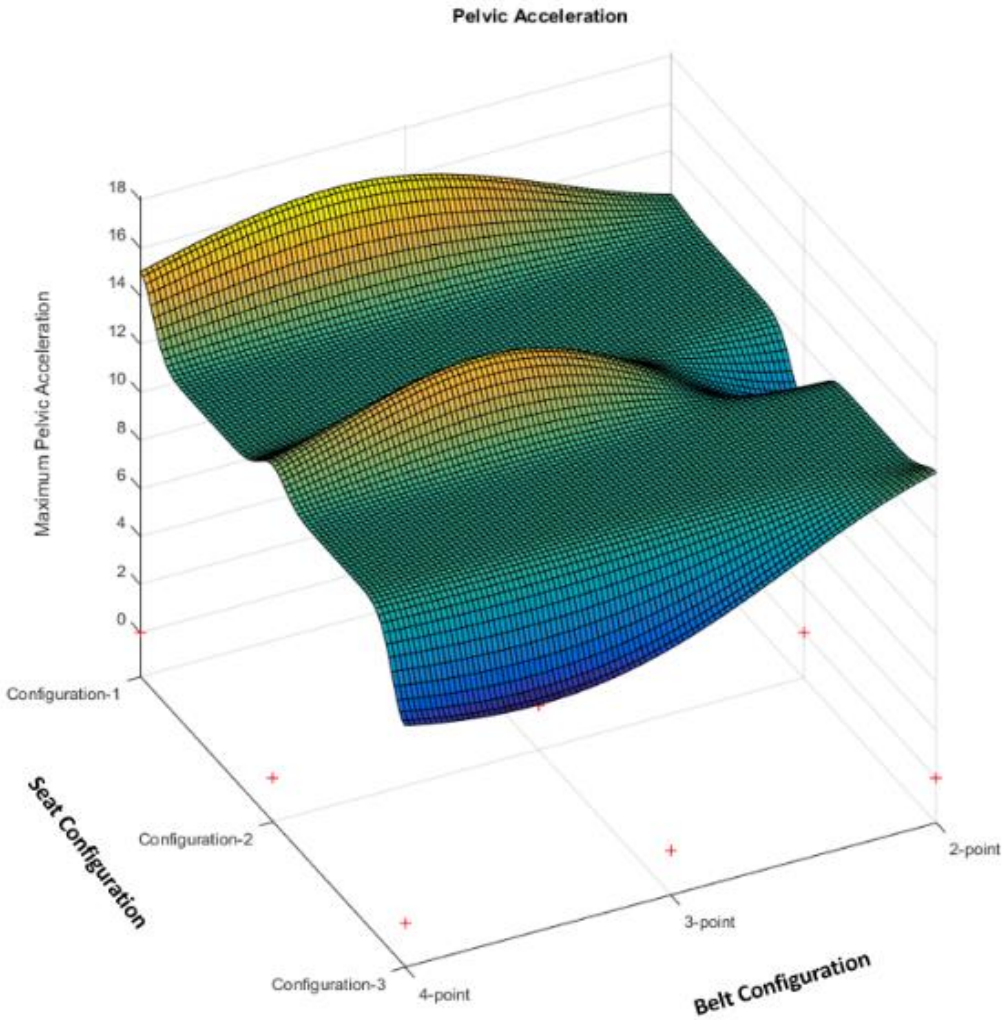

Figure 5.5 Surface Plot Showing Pelvis Acceleration.

5.3.3 Combined Plot

Figure 5.6 shows the surface plot, showing the variation of combined values (CP_D) with respect to Seat and belt configuration. All the parameters considered above are normalized by dividing the values with critical values and sum of all the parameters after division is multiplied to a scaling factor. The combined values therefore obtained are applied to the kriging model to generate this surface plot. It is very clear that the best results of all parameters put together is obtained from seat configuration-III and four-point belt system.

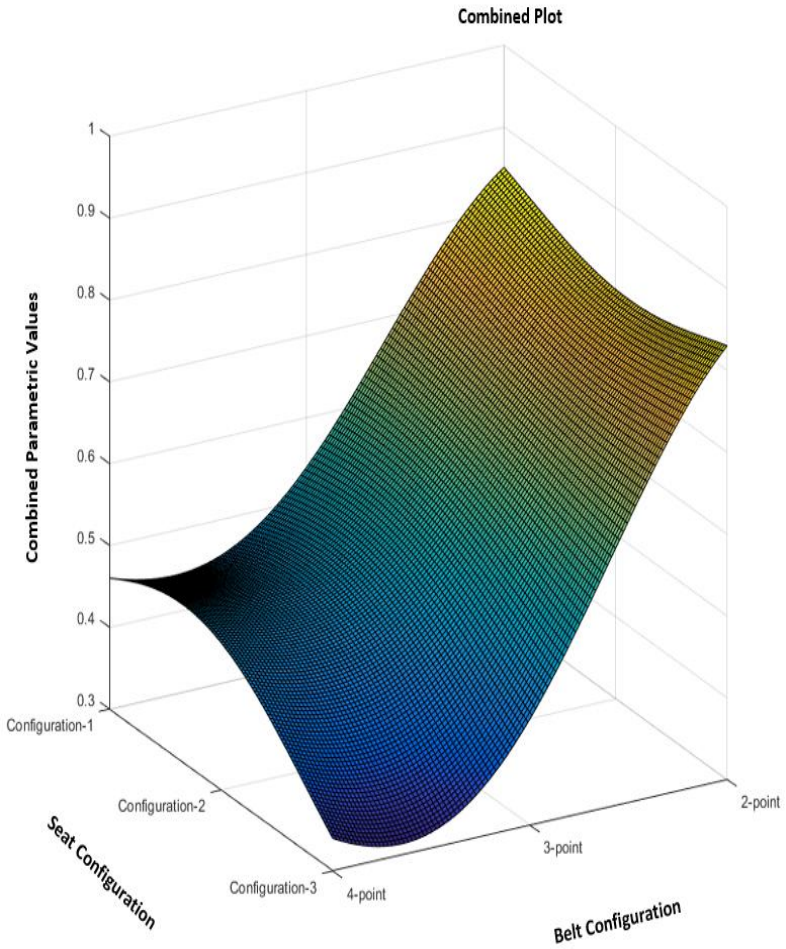

$$CP_D = \frac{1}{4}\left(\frac{F_B}{F_{BC}} + \frac{\Delta_H}{\Delta_{HC}} + \frac{F_L}{F_{LC}} + \frac{A_P}{A_{PC}}\right)$$

Where,

F_B = Belt forces

F_{BC} = Critical Belt forces

Δ_H = Head Excursion

Δ_{HC} = Critical Head Excursion

F_L = Lumbar Forces

F_{LC} = Critical Lumbar Forces

A_P = Pelvis Acceleration

A_{PC} = Critical Pelvis Acceleration

Figure 5.6 Surface Plot Showing Combined Values of All Considered Injury Parameters

5.4 Generated Surface Plots for Cornering, Test Condition-B (750mph)

Surface plots are generated for cornering condition of Test Condition-B (750mph). This is ideal situation having all probabilities of happening during a real-life hyperloop travel, except for the extreme radius of curvature. Therefore, studying this condition in detail has great significance.

5.4.1 Pelvic Acceleration During Cornering

Pelvic acceleration (A_P) variation during cornering with respect to different belt and seat configurations is shown in Figure 5.7. It can be observed that the value of pelvic acceleration is highest when two-point belt system used with seat configuration-I and also when seat three-point belt system is used with seat configuration-II. Though there is not a significant difference, best values are obtained while using four-point belt system in combination with seat configuration-III.

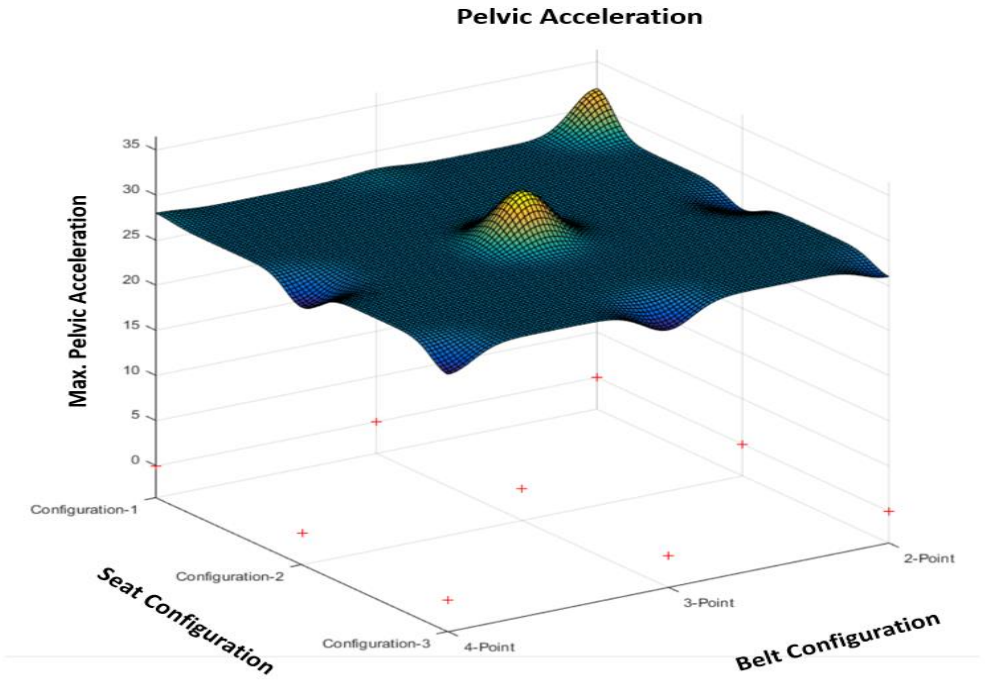

Figure 5.7 Surface Plot Showing Pelvis Acceleration.

5.4.2 Rib Deflection

Figure 5.8 shows the surface plot, showing the variation of rib deflection (RD) with respect to Seat and belt configuration. It is evident from the plot that, values corresponding to seat configuration-I is highest, irrespective of restraint system configuration utilized. Values corresponding to three-point and four-point belt systems do not vary considerably, but the least value is obtained from four-point system and Seat configuration-III.

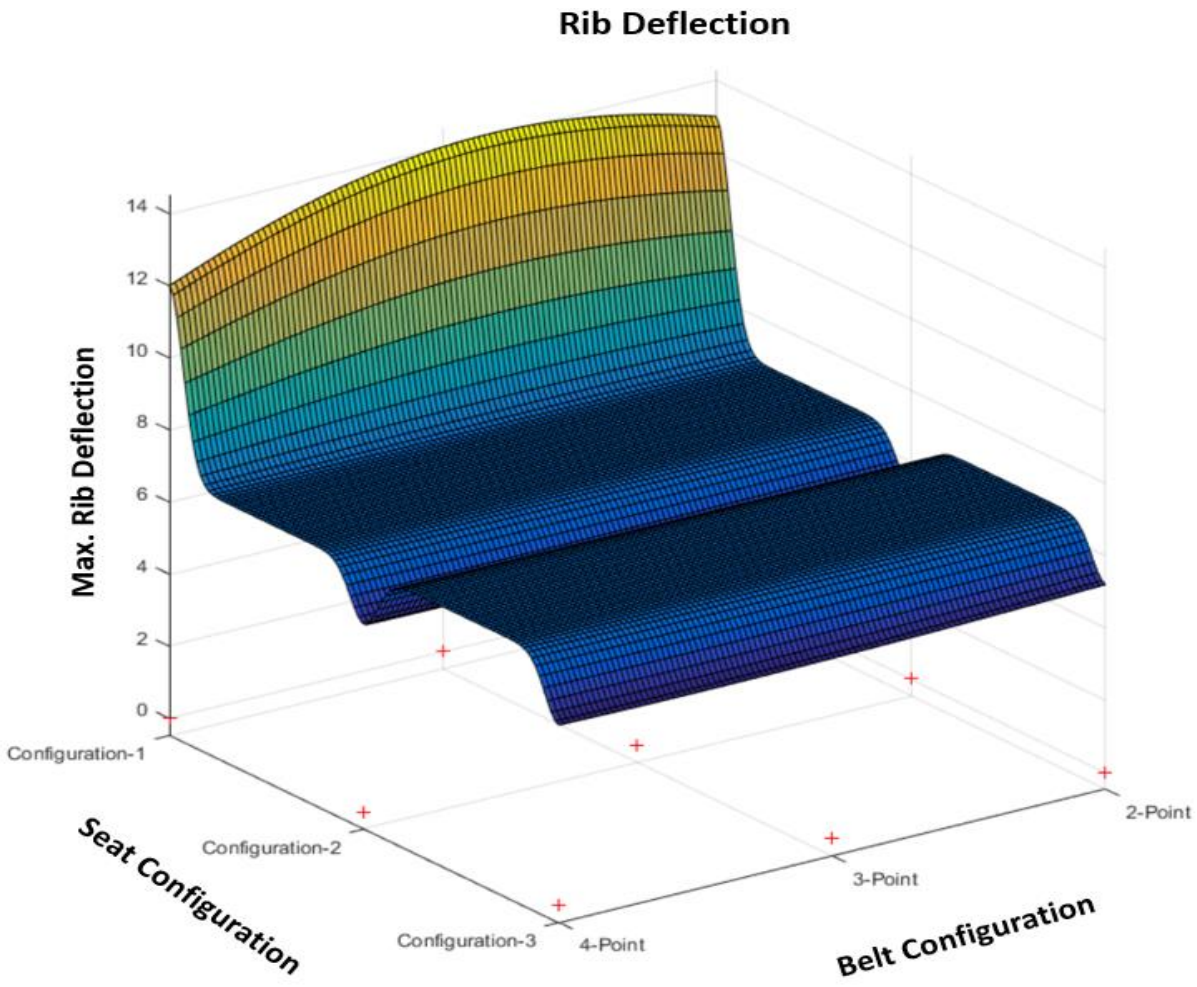

Figure 5.8 Surface Plot Showing Rib Deflection.

5.4.3 Viscous Criterion

Variation of viscous criterion (V*C) with respect to belt and seat configurations is shown in Figure 5.5. Viscous Criterion value corresponding to seat configuration-I and four-point belt system is the highest. Values obtained from three-point belt system corresponding to seat configuration-III and configuration-I is on the higher side. Least value of viscous criterion is the one corresponding to seat configuration-III and four-point belt system.

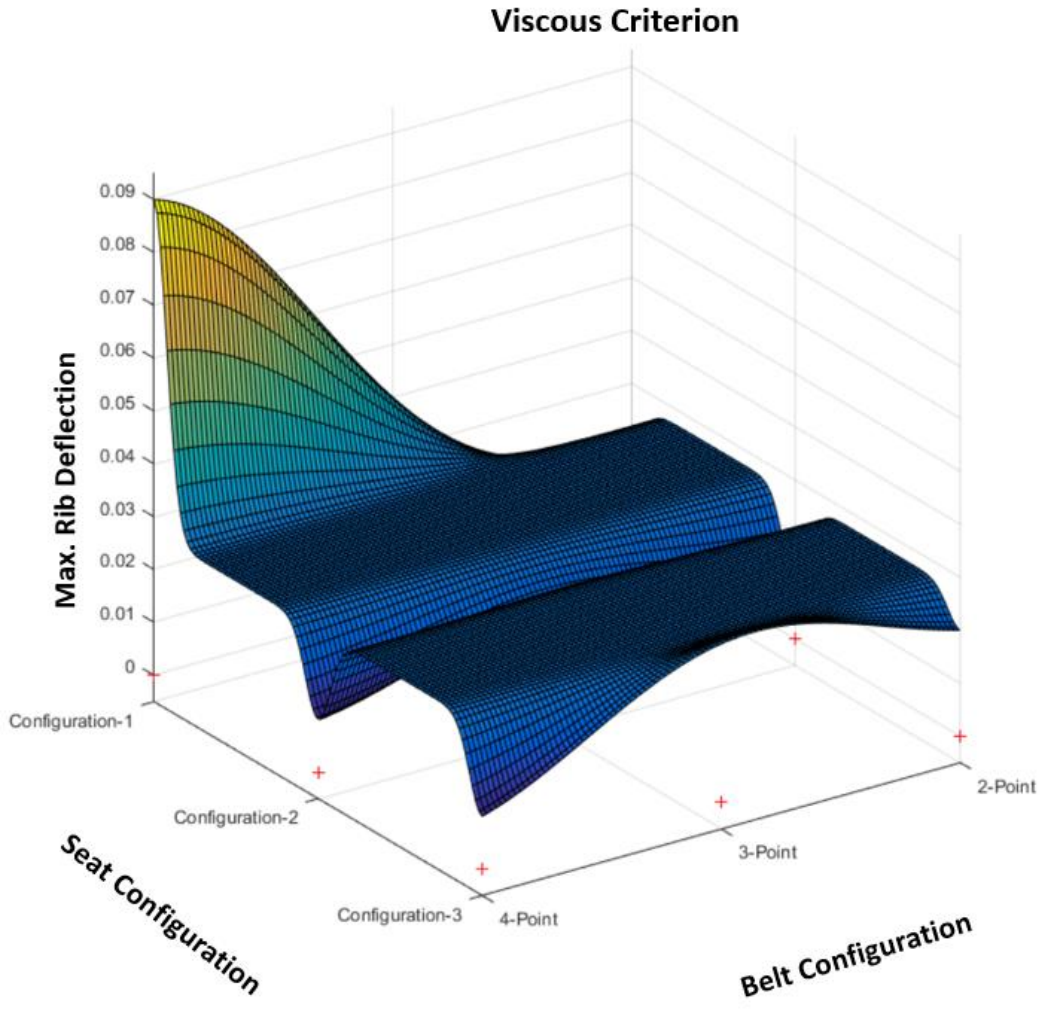

Figure 5.9 Surface Plot Showing Viscous Criterion.

5.4.4 Combined Plot (Cornering-750mph)

Figure 5.10 shows the surface plot, showing the variation of combined values (CP_C) with respect to Seat and belt configuration. All the parameters considered above are normalized in similar fashion as in the case of deceleration. The combined values therefore obtained are applied to the kriging model to generate this surface plot. It is very clear yet again that the best results of all parameters put together is obtained from seat configuration-III and four-point belt system.

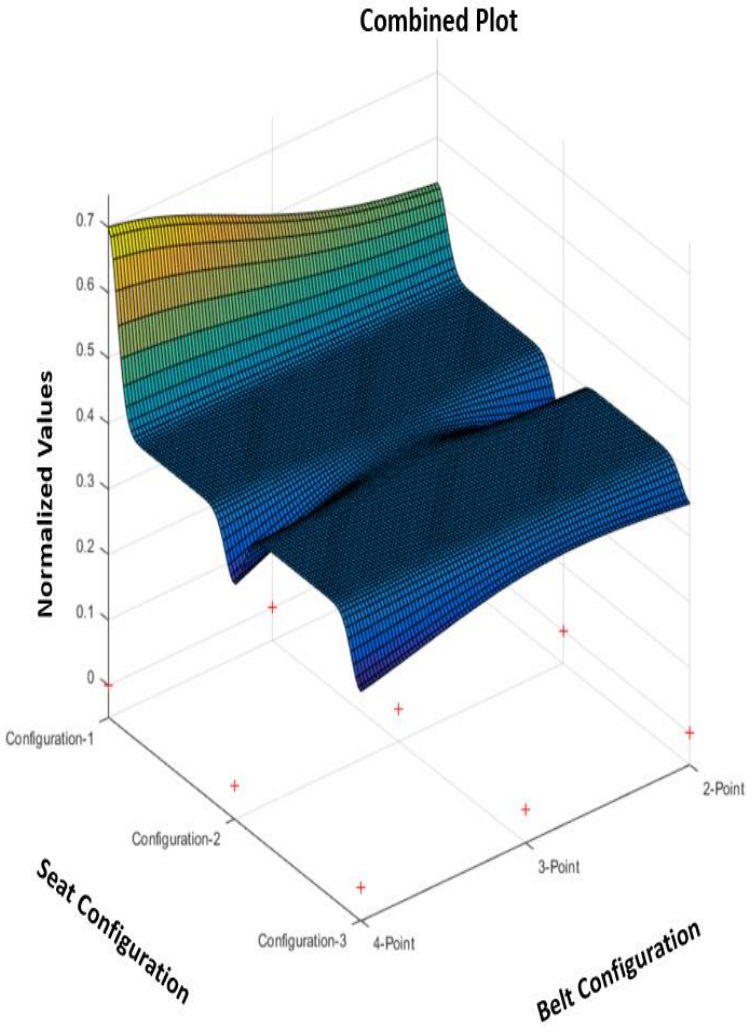

$$CP_C = \frac{1}{4}\left(\frac{A_P}{A_{PC}} + \frac{RD}{RD_C} + \frac{(V*C)}{(V*C)_C}\right)$$

Where,

A_P = Pelvis Acceleration

A_{PC} = Critical Pelvis Acceleration

$V * C$ = Viscous Criterion

$(V * C)_C$ = Critical Viscous Criterion

RD = Rib Deflection

RD_C = Critical Rib Deflection

Figure 5.10 Surface Plot Showing Combined Values of All Considered Injury Parameters

5.5 Average Combined Plot

Average of the combined values (C) obtained by normalizing parameters in deceleration and cornering conditions is calculated. These values can be relied upon to conclude on the best suited seat and belt configurations for both deceleration and cornering conditions. The values obtained are applied to the kriging model MATLAB code. Variation of the average values obtained with respect to belt and seat configurations is shown in Figure 5.11. As observed in majority of previous cases the best value is the one corresponding to seat configuration-III and four-point seat belt system.

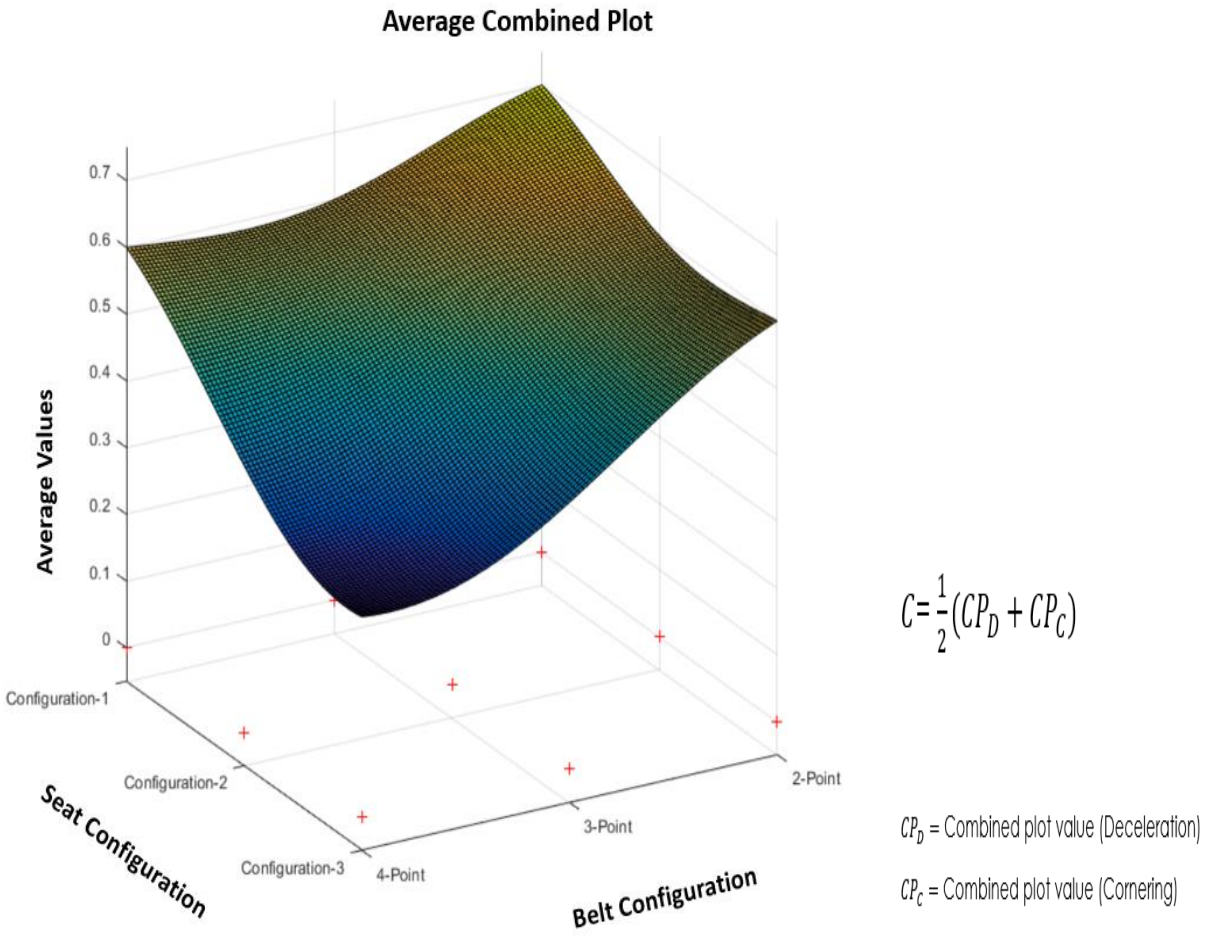

Figure 5.11 Surface Plot Showing Average Plot of Combined Values.

CHAPTER SIX

CONCLUSIONS AND RECOMMENDATION

6.1 Conclusions

The goal of this study was to study the effects of rapid acceleration on an occupant inside a Hyperloop capsule/pod. The behavior of an occupant under various acceleration, deceleration and cornering conditions was studied with the help of a Hybrid-III and Euro-SID 2re 50th percentile male dummies. Optimum seating and belt configuration was determined after studying the computational data obtained from the MADYMO.

6.1.1 Deceleration

It is clear from the kinematics and the data that in all the deceleration conditions considered in this study, not having safety restraints of any kind will lead to catastrophic head and neck injuries. Dummy in seating configuration-II and configuration-III experiences considerable increase in head acceleration values when compared to seat configuration-I, whereas pelvis acceleration values for configuration-III remained relatively lower at higher rates of acceleration. Lumbar loads remained in the same range for all the seat configurations with configuration-I having the best values. Configuration-II or III would be better in case of head excursion. Since the seats are inclined, probability of collision onto any structure in front can be considerably reduced. Seat configuration-III exhibited lower pelvic acceleration, lower belt loads, and considerably lumbar loads. Therefore, it was the best configuration during deceleration.

In comparison with the other belt configurations, the four-Point belt configuration showed best values in case of pelvic acceleration, minimal belt forces, lumbar resultant force and head acceleration. Therefore, seat configuration-III in combination with a four-point seat belt would be

the optimum configuration to minimize the effects of deceleration and probability of injury on an occupant.

6.1.2 Acceleration

While accelerating in Test Condition-A, seat configuration-I exhibited best values of head acceleration, lumbar resultant forces, pelvic acceleration, and belt forces, whereas while accelerating to much higher speeds in much lesser time configuration-II and III seemed to be better options. Acceleration during Test Condition-B and C takes its toll on the head, which is evident from the very high head acceleration values obtained. No seating or belt configuration seemed to be effective in case of the head acceleration in these scenarios and alternative measures might be needed to prevent this. With respect to other parameters, seat configuration-II and seat configuration-III seemed to be better options while accelerating to higher speeds.

Though there were no significant variation in the values of lumbar resultant forces and pelvis acceleration, four-point seat belt shows the best values. Therefore, seat configuration-II or seat configuration-III in combination with a four-point seat belt seemed to be the best seating and belt configurations during acceleration.

6.1.3 Cornering

Cornering at such high speed would not be an easy task to achieve. A turning radius of one mile was considered for this study. Kinematics indicated no seat belt simulations turning out to be catastrophic even in case of cornering. The values of head acceleration showed that the lateral acceleration caused due to cornering could lead to potential injuries. Increasing the radius of curvature would be the best bet to overcome this issue.

Seat configuration-III showed relatively better values of lumbar forces, pelvis acceleration. Though there is no significant difference in between the values obtained from three-point and four-point seat belts, a four-point belt would be better while traveling along curved paths. In case of a similar lateral acceleration being applied along the negative direction, a three-point belt would fail. Therefore, seating configuration-III in combination with a four-point belt would be ideal in a cornering scenario.

Considering acceleration, deceleration, and cornering, seat configuration-III along with a four-point belt is the best suited or optimal seating and belt configuration for the general safety of the occupant and to minimize probabilities of potential injuries. While utilizing this configuration, no structure should be placed in range of 70-75cm along the x-direction, to avoid any head collision in the event of a rapid deceleration.

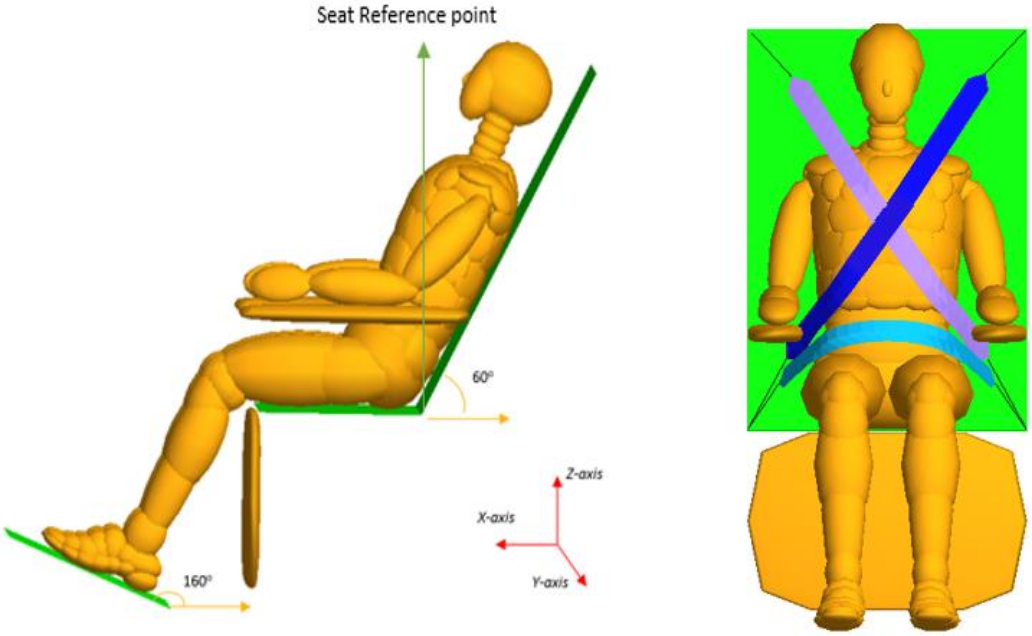

Figure 6.1 Best Suited Seat and Belt Configuration

6.2 Recommendations for Future work

Recommendations for further study on this topic:

- Various time spans and velocities can be considered, and the experiments can be repeated.
- ADAMS model of the pod travelling through a tube can be created and utilized to obtain more accurate acceleration pulses.
- Kinematics of deceleration and cornering scenarios showed probabilities of whiplash and head accelerations in certain cases being very high. Therefore, neck and head injury criteria can be studied.
- Various radii of curvature can be considered for cornering and the ideal radius of curvature can be determined.
- Effect of seat and belt properties on the parameters can be analyzed by applying various material properties to the seat and FE belts.
- Integrated seat belts or seat belts rigidly attached to the seats and their influences on injury parameters could be tested.

REFERENCES

REFERENCES

[1] Chin, J. C., Gray, J. S., Jones, S. M., & Berton, J. J. "Open-Source Conceptual Sizing Models for the Hyperloop Passenger Pod." In AIAA Science and Technology Forum, 56th AIAA/ASCE/AHS/ASC Structures, Structural Dynamics, and Materials Conference, Kissimmee, FL. (2015, January)

[2] King, A. I., Yang, K. H., Zhang, L., Hardy, W., & Viano, D. C. "Is head injury caused by linear or angular acceleration?" In IRCOBI conference (pp. 1-12). (2003, September)

[3] Rowson, S., & Duma, S. M. "Brain injury prediction: assessing the combined probability of concussion using linear and rotational head acceleration." *Annals of biomedical engineering*, 41(5), 873-882. (2013)

[4] Viano, D. C., Melvin, J. W., McCleary, J. D., Madeira, R. G., Shee, T. R., & Horsch, J. D. "Measurement of head dynamics and facial contact forces in the Hybrid III dummy." SAE Technical Paper. (No. 861891) (1986)

[5] Ewing, C. L., Thomas, D. J., Majewski, P. L., Black, R., & Lustick, L. "Measurement of Head, T 1, and Pelvic Response to-Gx Impact Acceleration" SAE Technical Paper (No. 770927). (1977)

[6] Ewing, C. L., Thomas, D. J., Lustik, L., Muzzy, W. H., Willems, G. C., & Majewski, P. "Dynamic response of the human head and neck to+ Gy impact acceleration" SAE Technical Paper. (No. 770928).1977.

[7] Taylor, C. L., Hyde, D. J., & Barr, L. C. "Hyperloop Commercial Feasibility Analysis." John A. Volpe National Transportation System Center. (2016)

[8] Östh, J., Brolin, K., Carlsson, S., Wismans, J., & Davidsson, J. "The occupant response to autonomous braking: a modeling approach that accounts for active musculature." *Traffic injury prevention*, 13(3), 265-277. (2012)

[9] Tay, Y. Y., Cai, Y., & Lankarani, H. M. 'Lumbar load estimation for a MADYMO FAA Hybrid-III scalable dummy." In ASME 2015 International Mechanical Engineering Congress and Exposition (pp. V012T15A011-V012T15A011). American Society of Mechanical Engineers. (2015, November).

[10] Lankarani, H. M., "Current Issue Regarding Aircraft Crash Injury Protection," Crashworthiness of Tranportation Systems: Structural Impact and Occupant, 1997.

[11] Lankarani, H. M., Ma, D., and Menon, R., "Occupant Dynamic Responses for Evaluation of Compliance Characteristics of Aircraft Bulkheads," 18th Annual ASME Design Automation Conference, 377-382, 1992.

[12] Ma, D., and Lankarani, H. M., "Computer Simulations of an Occupant-Restraint System," Proceedings: Teckfest 17 p 20 (See N 91-18004 10-01) 1991.

[13] Hooper, S. J., and Lankarani, H. M., "Application of Computer-Aided Analysis Tools for Aircraft Occupants and Seat Crashworthiness Problems," *International Journal of Crashworthiness*, 4(4), 443-448, 1999

[14] Lankarani, H. M., "Injury Bio-Mechanics Lecture," Wichita State University, 2016

[15] Prabhu, G., "Parametric study of Head Paths and HIC Data for Aircraft seat and Cabin Interior Certification," MS Thesis, Wichita State University, 2006.

[16] MADYMO reference manual, version 7.5, TASS INETRNATIONAL, [cited December 2017].

[17] VicHyper's Hyperloop, An artist's impression of VicHyper's Hyperloop, a finalist in the global SpaceX Hyperloop Pod competition, The Australian, 4 Oct. 2016 http://www.theaustralian.com.au/business/technology/hyperloop-highspeed-travel-is-coming--fast/news-story/3d043880f52d5f56c8a1433c137a100b [Cited, Dec 2017]

[18] Hyperloop One, Hyperloop One XP-1, Extreme tech, 3 Aug.2017 https://www.extremetech.com/extreme/253608-hyperloop-one-hits-almost-200-mph-demo-pod [Cited, Dec 2017]

[19] Teitel, A.S.(2014, September 26), John Paul Stapp, a Real Life Rocket (Sled) Man. Retrieved from https://www.popsci.com/blog-network/vintage-space/john-paul-stapp-real-life-rocket-sled-man [Cited, Dec 2017]

[20] Zhang, Z., Xu, L., Flores, P., Lankarani, H.M. "A Kriging model for dynamics of mechanical systems with revolute joint clearances". *Journal of Computational and Nonlinear Dynamics*. 2014 Jul 1;9(3):031013.

[21] Chakravarthy, N.V. P., "Development of response surface data on the head injury criteria associated with various aircraft and automotive head impact scenarios" (MS Thesis, Wichita State University), (2016)

[22] Mertz ,H. J., Prasad, P., Irwin, A. L. . "Injury risk curves for children and adults in frontal and rear collisions," in Proceedings of the 41st Stapp Car Crash Conference (Warrendale, PA: Society of Automotive Engineers) (1997)

[23] Kleiven, S. "Why most traumatic brain injuries are not caused by linear acceleration, but skull fractures are." Frontiers in bioengineering and biotechnology. 2013.

[24] Hutchinson, J., Kaiser, M.J., and Lankarani, H.M., "The Head Injury Criteria Functional," *Journal of Applied Mathematics and Computation*, Elsevier Sciences, Vol. 96, Issue 1, pp. 1-16, 1998.

[25] Lankarani, H.M., Gowdy, V., DeWeese, R., Kishore, P., Murthy, A., and Satish, S., "Kinematics of SID on Side-facing Aircraft Seats," *International Journal of Crashworthiness*, Vol. 3, No. 4, pp. 393-403, 1998.

[26] Lankarani, H.M., "Modeling Dynamic Responses of and Injury Potential to Occupants on Side-facing Aircraft Seats," Fourth Aircraft Fire and Cabin Safety Research Conference, Lisbon, Portugal, November 2004.

[27] Bhaskaran, B., Nagarajan, H., and Lankarani, H.M., "MADYMO Modeling of Occupant Dynamic Responses on Side-facing Aircraft Seats and Potential Neck Injuries," 5th MADYMO Users Meeting of America, Troy, Michigan, October 2003.

[28] Huculak, R.D., and Lankarani, H.M., "Methods of Evaluating ES-2 Leg Flail in Dynamic Evaluation and Certification Tests of Side-Facing Aircraft Seats," *International Journal of Crashworthiness*, Vol. 20, No. 6, pp. 613-628, 2015.

[29] Flores, F., and Lankarani, H.M., **Contact Force Models for Multibody Dynamics**, Scientific Book Published by Springer, "Solid Mechanics and Its Applications" Book Series, Vol. 226, 171p, ISBN: 978-3-319-30896-8, 2016. [DOI 10.1007/978-3-319-30896-5].

[30] Moradi, R., McCoy, M.L., and Lankarani, H.M., "Impact Analysis of Mechanical Systems Using Stress Wave Propagation Methodology," invited Book Chapter for the Book, **Wave Propagation**, L. Rocha and M. Gomes (Ed.), Academy Publish, ISBN: 978-09835850-X-X, pp. 211-249, 2014.

[31] Ma, D., Lankarani, H.M., "A Multibody/Finite Element Analysis Approach for Modeling of Crash Dynamic Responses," ASME *Journal of Mechanical Design,* Vol. 119, pp. 382-387, September 1997.

[32] Ma, D., Lankarani, H.M., "A Nonlinear Finite-Element Approach for Kineto-static Analysis of Multibody Systems," Fifth Conference on Nonlinear Vibrations, Stability, and Dynamics of Structures, Virginia Polytechnic Institute and State University, June 1994.

[33] Lankarani, H.M., and Menon, R., "Crash Responses of a Discrete-Parameter Model of the Human Head-Neck," 22nd Midwestern Mechanics Conference, pp. 481-483, University of Missouri-Rolla, October 1991.

[34] Lankarani, H.M., "Biomechanical Modeling and Simulations of the Human Body Motion," 8th International Conference on Mathematical and Computer Modeling, College Park, Maryland, April 1991.